



UNIVERSITY OF LEEDS

This is a repository copy of *Frontal and Lateral Submarine Lobe Fringes: Comparing Sedimentary Facies, Architecture and Flow Processes*.

White Rose Research Online URL for this paper:
<http://eprints.whiterose.ac.uk/107527/>

Version: Accepted Version

Article:

Spychala, YT, Hodgson, DM orcid.org/0000-0003-3711-635X, Prelat, A et al. (3 more authors) (2017) *Frontal and Lateral Submarine Lobe Fringes: Comparing Sedimentary Facies, Architecture and Flow Processes*. *Journal of Sedimentary Research*, 87 (1). pp. 75-96. ISSN 1527-1404

<https://doi.org/10.2110/jsr.2017.2>

© 2017 by the SEPM Society for Sedimentary Geology. This is an author produced version of a paper published in *Journal of Sedimentary Research*. Uploaded in accordance with the publisher's self-archiving policy.

Reuse

Unless indicated otherwise, fulltext items are protected by copyright with all rights reserved. The copyright exception in section 29 of the Copyright, Designs and Patents Act 1988 allows the making of a single copy solely for the purpose of non-commercial research or private study within the limits of fair dealing. The publisher or other rights-holder may allow further reproduction and re-use of this version - refer to the White Rose Research Online record for this item. Where records identify the publisher as the copyright holder, users can verify any specific terms of use on the publisher's website.

Takedown

If you consider content in White Rose Research Online to be in breach of UK law, please notify us by emailing eprints@whiterose.ac.uk including the URL of the record and the reason for the withdrawal request.



eprints@whiterose.ac.uk
<https://eprints.whiterose.ac.uk/>

1 **FRONTAL AND LATERAL SUBMARINE LOBE FRINGES: COMPARING SEDIMENTARY FACIES,**
2 **ARCHITECTURE AND FLOW PROCESSES**

3 YVONNE T. SPYCHALA^{1†*}, DAVID M. HODGSON¹, AMANDINE PRÉLAT², IAN A. KANE³ STEPHEN S.
4 FLINT³ and NIGEL P. MOUNTNEY¹

5 ¹*Stratigraphy Group, School of Earth and Environment, University of Leeds, LS2 9JT, UK*

6 ²*Beicip- Franlab, 232 Avenue Napoléon Bonaparte, 92500 Rueil-Malmaison, France*

7 ³*Stratigraphy Group, School of Earth, Atmospheric and Environmental Science, University of*
8 *Manchester, M13 9PL, UK*

9 [†]now at: Department of Earth Science, University of Utrecht, 3584 CS Utrecht, NL

10 **Corresponding author: Yvonne T. Sychala: y.t.sychala@uu.nl*

11 *Keywords: basin-floor lobes, frontal fringe, lateral fringe, facies distribution, flow transformation*

12

13

ABSTRACT

14 Submarine lobe fringe deposits form heterolithic successions that may include a high proportion of
15 hybrid beds. The identification of lobe fringe successions aids interpretation of paleogeographic
16 setting and the degree of basin confinement. Here, for the first time, the sedimentological and
17 architectural differences between frontal and lateral lobe fringe deposits are investigated. Extensive
18 outcrop and core data from Fan 4, Skoorsteenberg Formation, Karoo Basin, South Africa, allow the
19 rates and style of facies changes from axis to fringe settings of lobes and lobe complexes in both
20 down-dip (frontal) and across-strike (lateral) directions to be tightly constrained over a 800 km²
21 study area. Fan 4 comprises three sand-prone divisions that form compensationally stacked lobe
22 complexes, separated by thick packages of thin-bedded siltstone and sandstone intercalated with

23 (muddy) siltstone, interpreted as the fringes of lobe complexes. Lobe-fringe facies associations
24 comprise: i) thick-bedded structureless or planar laminated sandstones that pinch and swell, and are
25 associated with underlying debrites; ii) argillaceous and mudclast-rich hybrid beds; and iii) current
26 ripple-laminated sandstones and siltstones. Typically, frontal fringes contain high proportions of
27 hybrid beds and transition from thick-bedded sandstones over length-scales of 1 to 2 km. In
28 contrast, lateral fringe deposits tend to comprise current ripple-laminated sandstones that transition
29 to thick-bedded sandstones in the lobe axis over several kilometers. Variability of primary flow
30 processes are interpreted to control the documented differences in facies association. Preferential
31 deposition of hybrid beds in frontal fringe positions is related to the dominantly downstream
32 momentum of the high-density core of the flow. In contrast, the ripple-laminated thin beds in lateral
33 fringe positions are interpreted to be deposited by more dilute low-density (parts of the) flows. The
34 development of recognition criteria to distinguish between frontal and lateral lobe fringe
35 successions is critical to improving paleogeographic reconstructions of submarine fans at outcrop
36 and in the subsurface, and will help to reduce uncertainty during hydrocarbon field appraisal and
37 development.

38

39

INTRODUCTION

40 Traditionally, submarine lobe deposits are described as simple radial bodies that thin and fine from
41 an apex (e.g. Mutti, 1977; Normark, 1978; Lowe, 1982; Bouma, 2000). However, it has been
42 recognized from outcrop and geophysical studies that the anatomy of lobe deposits can be more
43 complicated in terms of facies distribution and geometry (e.g. Nelson et al., 1992; Twichell et al.,
44 1992; Bouma and Rozman, 2000; Gervais, 2006; Hodgson et al., 2006; Deptuck et al., 2008; Pr lat et
45 al., 2009; Groenenberg et al., 2010; Etienne et al., 2012). Pr lat et al. (2009) proposed four sub-
46 environments for lobe deposits that are characterized by specific facies associations and thickness
47 trends, termed lobe axis, lobe off-axis, lobe fringe and lobe distal fringe (Fig. 1a).

48 Placing constraints on the temporal and spatial variability of lobe fringe successions is important to
49 help improve reconstructions of deep-water fans, and to provide suitable building blocks for
50 reservoir modelling and to reduce uncertainty in the evaluation of subsurface stratigraphic traps
51 (e.g. Biddle and Wiechowsky, 1994; Etienne et al., 2012; Bakke et al., 2013; Collins et al., 2015;
52 Grecula et al., 2015). Hybrid beds (e.g. Haughton et al., 2003; Talling et al., 2004; Haughton et al.,
53 2009; Davis et al., 2009) and heterolithic deposits dominated by thin-bedded turbidites, have been
54 associated with lobe fringe environments (Ito, 2008; Hodgson, 2009; Talling et al., 2012a; Etienne et
55 al., 2012; Grundvåg et al., 2014; Patacci et al., 2014; Collins et al., 2015; Fonnesu et al., 2015, Porten
56 et al., 2016; Southern et al., 2016). Previous work on lobe fringe successions has focused on pinch-
57 out geometries (e.g. Rozman, 2000; Marini et al., 2011; Etienne et al., 2012; Nagatomo and Archer,
58 2015). Some authors (e.g. MacPherson, 1978; Pickering, 1981, 1983) have documented differences
59 between down-dip and across-strike facies transitions in lobe deposits. However, detailed
60 depositional architecture, recognition criteria and facies variability between down-dip (frontal) and
61 across-strike (lateral) lobe fringe environments remain poorly constrained.

62 The aim of this integrated outcrop and core study is to assess the difference between frontal and
63 lateral lobe fringe successions using the paleogeographically well-constrained Fan 4 succession of
64 the Skoorsteenberg Formation, Karoo Basin, South Africa. Specific research objectives are as follows:
65 1) to establish the characteristic facies associations that distinguish the different lobe fringe settings;
66 2) to interpret flow processes that produce the observed facies variability; 3) to discuss the role of
67 confinement in the distribution and character of lobe fringes; and 4) to assess the implication of the
68 results for subsurface applications.

69 **GEOLOGICAL SETTING**

70 The Karoo Basin has been interpreted as a retroarc foreland basin connected to a magmatic arc and
71 fold-thrust belt (Cape Fold Belt) (Visser & Prackelt, 1996; Visser, 1997; Catuneanu et al., 1998).
72 Alternatively, Tankard et al. (2009) argue that subsidence during the early, deep-water, phase of

73 deposition, which is the focus of this study, pre-dates the effects of loading by the Cape Fold Belt,
74 and was induced by dynamic topography associated with mantle flow processes coupled to distant
75 subduction of the paleo-Pacific plate (Pysklywec & Mitrovica, 1999). The basin-fill comprises the
76 Karoo Supergroup and records sedimentation from Late Carboniferous to Early Jurassic. The Karoo
77 Supergroup comprises the glacial Dwyka Group, the deep- to shallow-marine Ecca Group and the
78 non-marine (fluvial) Beaufort Group. The Ecca Group, which is the focus of this study, represents a
79 shallowing-upward succession of sediments from deep-water to fluvial settings (Flint et al., 2011).

80 The Tanqua depocentre is located in the southwest of the Karoo Basin adjacent to the Cederberg
81 branch of the Cape Fold Belt (Fig. 2a). Here, the Lower Ecca Group comprises the Prince Albert
82 Formation (shallow-marine), the Whitehill Formation (deep-marine) and the Collingham Formation
83 (deep-marine); the Upper Ecca Group comprises the Tierberg Formation (basin-plain), the
84 Skoorsteenberg Formation (basin-floor to base-of-slope), the Kookfontein Formation (slope to shelf-
85 edge) and the Waterford Formation (shoreface) (Fig. 2b; Bouma & Wickens, 1991; Wickens, 1994).

86 The Skoorsteenberg Formation (250 m thick; Bouma & Wickens, 1994) is subdivided into five sand-
87 prone bodies. The lower four sandstone bodies (Fans 1-4) have been interpreted as basin-floor fans
88 (Morris et al., 2000; Wickens & Bouma, 2000, Johnson et al., 2001), whereas the fifth (Unit 5) has
89 been interpreted as a lower slope to base-of-slope system (Wickens & Bouma, 2000; Wild et al.,
90 2005; Hodgson et al., 2006). Although a submarine fan represents a system built up by channels and
91 lobes, the term 'Fan' is retained here as a lithostratigraphic descriptor for consistency with previous
92 literature. Fans 1-4 are each up to 65 m thick, with gradational to sharp bases and tops (Johnson et
93 al., 2001) separated by claystones and siltstones (Van der Werff & Johnson, 2003a). Each fan is
94 interpreted as a lowstand systems tract, with the overlying fine grained deposits of regional extent
95 representing the related transgressive and highstand systems tracts (Goldhammer et al., 2000;
96 Johnson et al., 2001; Hodgson et al., 2006; Hodgson, 2009).

97 This study focuses on the lobe deposits of Fan 4, a lobe complex-set (Fig. 1b), in an 800 km² study
98 area (Fig. 2a). Fan 4 is up to 65 m thick (Johnson et al., 2001) and is characterized by a high degree of
99 amalgamation in the Skoorsteenbergs area (Fig. 3; Dudley et al., 2000). Paleocurrents and thickness
100 distributions indicate that sediment was sourced from both the southwest and west (Dudley et al.,
101 2000; Hodgson et al., 2006), in contrast to the underlying fans (Fans 1-3) that are point sourced from
102 the SW. General paleocurrent orientations are to the east and northeast (Wickens & Bouma, 2000;
103 Hodgson et al., 2006). Fan 4 is divided into two sand-rich units named the lower and upper
104 sandstone divisions (Wickens & Bouma, 2000; Hodgson et al., 2006) separated by a thin-bedded
105 siltstone package that is up to 6 m thick in the south and thins and fines northward. The upper
106 division thickens to the north where the lower division thins, which was suggested by Hodgson et al.
107 (2006) to indicate compensational stacking. The stratigraphy of Fan 4 has been revised to show that
108 the lower sandstone division comprises one sand-prone lobe complex, whereas the upper division
109 comprises two sand-prone lobe complexes, separated by thin-bedded heterolithic lobe complex
110 fringe strata.

111

112

METHODOLOGY

113 For this study, 24 sections were measured in strategically chosen locations (Fig. 3) in order to collect
114 a data set that provides 3-D constraints. Graphic sedimentary logs record lithology, paleocurrent and
115 bed thickness data. Detailed bed-by-bed sections (see section locations on Fig. 3; ranging from 3 to
116 60 m in length and totaling 510 m in cumulative thickness) record grain size, sedimentary structures
117 and bounding surfaces of beds. Logs were recorded at 1:25 scale in the field. Four newly drilled,
118 near-outcrop cores (see well locations on Fig. 3) intersect Fan 4 (212 m total thickness) and were
119 logged at 1:4 scale. These data were augmented with three core logs (see locations of NOMAD –

120 Novel Modelled Architecture of Deepwater reservoirs – project; wells on Figure 3; 128 m cumulative
121 thickness) and 19 graphic logs collected during previous research (Hodgson et al., 2006; Prélat et al.,
122 2009) (Fig. 3). Outcrop sections and core logs were redrawn at 1:50 scale for correlation purposes.
123 The base of the mudstone and siltstone interval that separates the lower and upper sandstone
124 division of Fan 4 was used as a correlation datum. Paleocurrent measurements (108 in total) were
125 collected from current-ripple and climbing-ripple laminated sandstones, and flutes and grooves
126 preserved as casts on bed bases. To determine facies associations and architectures of frontal and
127 lateral fringe deposits at the scale of individual lobes, the hierarchy and paleogeography of Fan 4
128 was revised to improve the spatial understanding of lobe distribution.

129

130

MODEL OF LOBE ANATOMY

131

Hierarchy

132 A five-fold hierarchy of lobes in the Tanqua was proposed by Prélat et al. (2009): 1) a ‘bed’
133 represents a single depositional event; 2) one or more beds form a ‘lobe element’; 3) several lobe
134 elements that are divided by thin siltstone intervals stack to form a ‘lobe’; 4) one or more lobes stack
135 to form a ‘lobe complex’ (Fig. 1b). The hierarchy can be extended to the ‘lobe complex set’, which is
136 formed by the stacking of one or more related lobe complexes within the same lowstand systems
137 tract (Fig 1b). Prélat and Hodgson (2013) demonstrated that extensive meter-thick, thin-bedded
138 units between sand-rich lobes, originally referred to as ‘interlobes’ by Prélat et al. (2009), represent
139 the distal fringes of lobes. Typically, these are separated from sand-rich lobe deposits (axis and off-
140 axis) across an abrupt surface interpreted to mark an up-dip channel avulsion (Prélat and Hodgson,
141 2013). Thicker and more extensive thin-bedded successions can be interpreted as the fringes of lobe
142 complexes (Prélat and Hodgson, 2013).

143

Sedimentary facies and facies associations

144 Aspects of the sedimentary facies and related environments of deposition of the Skoorsteenberg
145 Formation have been described in detail previously (e.g. Morris et al., 2000; Johnson et al., 2001; van
146 der Werff and Johnson 2003; Hodgson et al., 2006; Luthi et al., 2006; Pr lat et al., 2009; Hodgson,
147 2009, Jobe et al., 2012; Hofstra et al., 2015). Individual facies encountered in both outcrop (Fig. 4a-f)
148 and core (Fig. 5a-f) datasets are summarized in Table 1. The facies combine into common facies
149 associations representing different lobe environments: lobe axis, lobe off-axis, lobe fringe and lobe
150 distal fringe (Pr lat et al., 2009; Fig. 1a). The boundaries between these environments are
151 transitional. This fourfold division has been applied to several outcrop studies (e.g. Etienne et al.,
152 2012; Pr lat and Hodgson, 2013; Grundv g et al., 2014; Spsychala et al., 2015; Marchand et al., 2015;
153 Masalimova et al., 2016). Lobe dimensions from several studies of sand-rich systems (Jegou et al.,
154 2008; Saller et al., 2008; Deptuck et al., 2008; Pr lat et al., 2009; S mme et al., 2009) show that
155 these bodies have elongate shapes with length-to-width ratios of 1.7 – 3.6 (Pr lat et al., 2010).
156 Average dimensions of lobes in the Tanqua depocentre are 27 km (length) \times 13 km (width) \times 5 m
157 (thickness) (Fan 3, Pr lat et al., 2009). Similar dimensions are expected for the lobes of Fan 4 as it
158 was deposited under similar conditions (e.g. relatively unconfined, similar grain-size range), and
159 similar lobe dimensions are identified across different unconfined systems (Pr lat et al., 2010).

160 **Lobe axis.**---Lobe axis deposits are dominated by thick-bedded, structureless sandstone (F1; Figs. 4a,
161 5a; Table 1) with subordinate planar laminated (F2; Figs. 4b, 5b; Table 1) and banded sandstone (F3;
162 Fig. 5c; Table 1) in minor proportions. The lobe axis setting is characterized as 85–100% sandstone.
163 Multiple zones of amalgamation occur across strike (Pr lat et al., 2009) and can form packages up to
164 5 m thick where there is scouring at the base of the lobe. The deposits of the lobe axis are laterally
165 extensive down-dip and across strike for several hundred meters, and generally show tabular
166 geometries (Fig. 4a). Units of high amalgamation can be traced into well-bedded units of the lobe
167 off-axis towards the frontal and lateral margin of the lobe deposits.

168 **Lobe off-axis.**---Lobe off-axis deposits comprise well stratified medium-bedded structured sandstone
169 (F2; Table 1) and are typically 2 to 4 m thick. Lobe off-axis deposits are characterized by 50–85%
170 sandstone. They show tabular geometries in outcrop and can be traced out for several hundred
171 meters in both dip and strike directions.

172 **Lobe fringe.**---Lobe fringe deposits comprise a range of facies, including structureless sandstone (F1),
173 hybrid beds (F4; Figs. 4c,d; Table 1), debrites (F5; Fig. 5e; Table 1) and heterolithic packages (F6; Figs.
174 4d, 5e; Table 1). Lobe fringe deposits are characterized by 20–50% sandstone. Typical thicknesses
175 range between 0.1 and 2 m. Several meter-thick successions (>2 m) are interpreted as fringes to lobe
176 complexes; such accumulations can be walked out into thick lobate sandstone units without
177 truncation (cf. Pr elat and Hodgson, 2013). At outcrop, lobe fringe deposits can show either tapering
178 or pinch-and-swell geometries. The pronounced pinch-and-swell geometries form lenticular bodies,
179 even though no evidence of truncation is observed (Bouma and Rozman, 2000; Groenenberg et al.,
180 2010). The lateral extent of lobe fringe deposits is variable and ranges from a few to several
181 kilometers. The transition from lobe fringe to lobe distal fringe environment marks the sand pinch-
182 out of the system.

183 **Lobe distal fringe.**---The lobe distal fringe environment is dominated by thin-bedded siltstone
184 deposits (F7; Figs. 4e; 5g; Table 1). Some thin very fine-grained sandstone beds are intercalated in
185 these siltstone-prone packages (<20% sandstone). Siltstones can aggrade to form bedded
186 successions of several meters in thickness. Lobe distal fringe deposits form an extensive ‘halo’
187 around the main sand-prone lobe body and extend for several kilometers. Their dimensions have not
188 been established.

189 In summary, lobe axis and off-axis deposits build the core of a lobe body and are dominated by
190 structureless and structured sandstone. Sandstone percentage decreases towards the lobe fringe
191 and is lowest in distal lobe fringe environments.

192

193

ARCHITECTURE

194

Thickness distribution and paleoflow directions

195 Fan 4 is subdivided into a lower and upper sand-prone division, separated by a thin-bedded
196 heterolithic division (Fig. 6, 7a). The two sand-prone divisions of Fan 4 show different thickness
197 trends and paleocurrent patterns.

198 The lower, sand-prone division has a maximum thickness of ~25 m in the southern part of the study
199 area (Fig. 6). Thinning is documented to the north and the northeast. The lower division records
200 paleoflow to the northeast but this trend is more northwards in the northern part of the study area
201 (Fig. 6). Correlation panels (Fig. 7) show that down-dip pinch-out of lobe deposits occurs in several
202 areas, such as around BK, NB2, GBE, OC7 and los6 area (Fig. 7). The final sand-pinch out to the
203 northeast occurs in the Vaalfontein- Sout Rivier area (Fig. 3). Notable lateral thinning across strike
204 towards the east (NS3) can be observed (~5.5 m/km). Thin (< 2 m thick) siltstone deposits are
205 deposited farther to the north where they thin gradually.

206 The thin-bedded heterolithic division that separates the lower and upper sand-prone divisions of Fan
207 4 thins and fines over 30 km from Bizansgat in the S (~6 m) gradually to Sout Rivier in the N (~0.7 m)
208 (Fig. 8).

209 The upper sand-prone division of Fan 4 has more complicated facies, thickness and paleoflow
210 distributions. There are two areas that show high thickness values (Fig. 6). Maximum thickness in the
211 southern study area is ~35 m (Bizansgat) from where the division thins to the north and northeast,
212 with paleoflow trends that conform to the northeasterly to northerly trends of the lower division
213 and of underlying Fan 3 (cf. Wickens and Bouma, 2000; Hodgson et al., 2006; Pr elat et al., 2009). In
214 the area around Skoorsteenbergr, the upper division is 47 m thick (Fig. 6) with paleoflow trends that
215 record a radial spread of directions from the northeast to southeast (Fig. 6; cf. Hodgson et al., 2006).

216 A laterally extensive ~3 m thick extensive thin-bedded unit is present towards the top of the upper
217 division. Thinning also occurs to the northeast and southeast, with the rate of thinning to the
218 northeast being highest (~6.9 m/km). The most northeastern outcrops around Katjiesberg (down-
219 dip) record dominantly northward paleocurrents and are characterized by highly variable
220 thicknesses, which range between 2 and 14 m and reflect a pinching and swelling trend of the
221 deposits (Fig. 6b). Correlation panels (Fig. 7) show that the oldest deposits pinch-out in the Sout
222 Rivier area, and the youngest deposits do not reach as far as the Katjiesberg area; therefore, an
223 overall basinward to landward stacking pattern is constrained.

224

225 *Hierarchy of Fan 4*

226 Thicknesses, facies associations and paleocurrents indicate that the lower division of Fan 4
227 comprises one lobe complex (Fig. 8a, LC1) that was fed by flows from the southwest. The heterolithic
228 succession that separates the lower and upper sand-prone divisions of Fan 4 comprises thin-bedded
229 silty mudstone, siltstone and sandstones (heterolithic deposits) (Fig. 8b, c). The facies association,
230 the lack of hemipelagic claystone, and the thickness patterns, collectively suggest this succession
231 most-likely represents the distal fringe of a lobe complex (cf. Pr lat et al., 2009). The associated
232 sand-prone deposits of this lobe complex (LC2) are inferred to have been located to the west,
233 beyond the outcrop exposure. Paleoflow and thickness trends suggest two distinct sediment entry
234 points for the upper sand-prone division of Fan 4 (Wickens & Bouma, 2000; Dudley et al., 2000;
235 Hodgson et al., 2006). The upper part of Fan 4 comprises two sand-prone lobe complexes (LC3 and
236 LC5). They both have maximum thicknesses in the Skoorsteenbergs area, and are separated by a ~3 m
237 thick extensive thin-bedded unit that is interpreted as the fringe of another lobe complex (LC4; Fig.
238 8a).

239 *Facies distribution*

240 Successive lobe deposits in weakly confined settings build lobe complexes that commonly exhibit
241 compensational stacking patterns driven by avulsion of distributive channels (Pickering, 1981;
242 Deptuck et al., 2008; Pr lat et al., 2009; Pr lat and Hodgson, 2013) (Fig. 9a-d). The distribution of
243 sedimentary facies are described from LC1 (lower division; Fig. 10) and LC 3-5 (upper division; Fig.
244 10b).

245 In the southern part of the study area, where LC1 is thickest, the deposits are dominated by
246 structureless (F1) and structured sandstone (F2; see Table 1; $F1+F2 > 75\%$) (Fig. 10). The proportion
247 of hybrid beds (F4) increases northwards where they can represent up to 50% of the thickness (e.g.
248 Vaalfontein; Fig. 3). Heterolithic deposits (F6) dominate the basal part of LC1 around the NB2, NS2
249 and NS1 well locations (Fig. 3). The NS3 well is represented by heterolithic deposits ($\sim 70\%$), siltstone
250 ($\sim 10\%$) and mudstone ($\sim 20\%$) (Fig. 11). Structureless sandstones are present in the northern part of
251 the study area in highly variable proportions (15% to 50% of deposits) (Fig. 10a). Sandstone-pinch-
252 out of the lobe complex occurs in the Sout Rivier area (Fig. 7). Northwards, the deposits of LC1
253 consist entirely of thin-bedded siltstones.

254 The upper part of Fan 4, which comprises LC3, LC4, and LC5, is characterized by a higher proportion
255 of structureless sandstone. The southern study area is marked by structureless (F1), structured (F2)
256 and banded sandstones (F3), which represent the bulk of deposits (50% to 75%). Hybrid beds (F4)
257 contribute 20% of the facies composition in Koppieskraal; elsewhere they contribute less than 10%.
258 Heterolithic deposits (F6) contribute 15% to 35% towards the central study area but less than 10% in
259 the southern study area. The northern study area is dominated by structureless sandstone deposits
260 (more than 50%) with the highest proportion observed in the Skoorsteenberg area (up to 80%).
261 Structured sandstone is a minor contributor ($\sim 15\%$). Hybrid beds represent less than 10% of
262 deposits, and heterolithic deposits commonly represent 10% to 15%. In the Katjiesberg area in the
263 northeast, almost no heterolithic deposits are present ($< 2\%$) but thin-siltstone deposits are
264 intercalated with structureless sandstone and hybrid beds.

265

266

Fan 4 paleogeographic reconstruction

267 Integration of paleoflow and thickness trends with facies distribution enables reconstruction of the
268 lower (LC1) and upper (LC3-5) divisions of the Fan 4 lobe complex set (Fig. 10). Paleoflow directions
269 for LC1 are both to the north and northeast (Fig. 6), whereas sediment entered from the southwest
270 (e.g. Dudley et al., 2000; Hodgson et al., 2006). This suggests that the northward pinch-out
271 represents a frontal fringe and the eastern termination a lateral pinch-out at the scale of the lobe
272 complex (Fig. 7). Younger lobe deposits of LC1 pinch-out successively farther to the north, which is
273 consistent with a progradational stacking pattern (*sensu* Hodgson et al., 2016), and frontal pinch-out
274 at the scale of a lobe. The frontal sand pinch-out of LC1 in the Sout Rivier area (Fig. 2) is associated
275 with a pinch-and-swell geometry of lobes and predominantly structureless sandstone and hybrid
276 beds (Fig. 7). A 'halo' of thin-bedded siltstone, which represents distal lobe fringe deposits, is
277 deposited farther to the north. Deposits across strike (lateral) to the east are dominated by
278 heterolithic deposits (NS3; Figs. 10, 11). The change in facies is associated with thinning of LC1.
279 Therefore, the deposits observed in NS3 represent several lateral lobe fringes that stack to form the
280 lobe complex fringe. Similar facies changes have also been identified on the western margin of LC1
281 by Hodgson et al. (2006) in the Los Kop area (marked in Fig. 10).

282 The upper division of Fan 4 comprises two sand-rich lobe complexes, LC 3 and LC5, separated by an
283 extensive thin-bedded heterolithic interval interpreted as the lobe complex fringe, LC 4. LC3 has two
284 thick and axial zones, in the Bizansgat and in the Skoorsteensberg area (Fig. 9). The facies
285 distribution patterns and paleoflow (Fig. 6) indicate that deposition could have been by two coeval
286 systems with different entry points. This interpretation is supported by the lack of clear trends in
287 facies distributions over the study area pointing to a complicated interaction of depositional systems
288 in the south and north. The deposits are treated as a single lobe complex because no bounding
289 surface or extensive thin-bedded units separating the two thick and axial areas have been observed

290 that could have been the result of avulsion. Generally, facies distributions suggest that, in the
291 southern part of LC3, there was compensational stacking of lobes as heterolithic intervals with
292 hybrid beds alternate with packages of structured and structureless sandstones across abrupt
293 surfaces in vertical sections. The northern part of LC3 and LC5 show dominantly aggradational
294 stacking patterns of lobes (Fig. 9). Facies changes (e.g. F1 and F3) can be explained by
295 compensational stacking on lobe element-scale (Prélat et al., 2009; Etienne et al., 2012; Prélat &
296 Hodgson, 2013) and scouring and amalgamation of lobe axes. Abrupt facies changes from
297 heterolithic deposits (distal lobe fringes) to sand-prone lobes suggest sufficient space for lateral
298 compensation. In the down-dip direction (Katjiesberg) of LC3, structureless sandstone, siltstone and
299 hybrid beds that show pinch-and-swell geometries dominate the lobe complex (Fig. 13, 14). These
300 are interpreted as stacked frontal lobe fringe deposits. The low proportion of hybrid beds otherwise
301 in the northern part of LC3 reflects the complicated 3D geometry of individual lobes. Integration of
302 paleocurrents and isopach maps would predict that a higher proportion of hybrid beds may be found
303 in the subcrop to the east. Due to the complexities in LC3 and the fragmented outcrop record of LC5,
304 the architecture of lobes, from their axes to their fringes has focused on LC1. The results can be
305 applied to the younger lobe complexes where data constraints permit.

306

307

LOBE FRINGE ASSOCIATIONS

308 Paleogeographic reconstruction of the Fan 4 lobe complex 1 (LC1) shows that lateral and frontal lobe
309 fringe environments can be well constrained in a lobe complex using isopach maps and
310 paleocurrents (Fig. 10). Integration of these data with mapped sand pinch-outs enables the relative
311 position and orientation of individual lobe bodies to be determined with confidence (Fig. 10).
312 Generally, their dip direction is to the N, whereas their strike direction is to the E and W. Figure 12
313 depicts characteristic transitions in facies at lateral (Fig. 12a) and frontal (Fig. 12b) lobe fringes in

314 LC1, which are described in detail below. Frontal and lateral lobe fringe environments are shown to
315 display characteristic facies associations and geometries that are summarized in Table 2.

316

317 *Lateral lobe fringe*

318 Figure 12a shows a correlation panel of a single lobe from Hammerkranz to NS2 in LC1 (Figs. 3 and
319 10a). The lobe is defined by sharp lower and upper changes in facies to distal lobe fringe successions.
320 Using the well-constrained paleogeographic map of LC1, this is a lateral transition from axial lobe
321 deposits (dominated by F1 and F2) to a succession that is dominated by structured sandstone and
322 heterolithic deposits. The lobe thins from 5.5 m in the axial position to 1.9 m in the lateral position in
323 4 km (0.9m/km rate of thinning). The lower part of the lobe exhibits a transition into thin-bedded
324 lobe fringe deposits, and the upper part of the lobe exhibits a transition to traction dominated
325 sandstones. Bed amalgamation is not observed.

326 The NS3 core (Fig. 11) shows an example of the lateral margin of a lobe complex (LC1) where all
327 lobes pass stratigraphically into an aggradational stack of fringe deposits. The integration of
328 observations of the detailed facies transition and the lobe fringe-dominated succession in NS3 allows
329 the following characteristics for lateral lobe fringes to be established. The lateral lobe facies
330 association is dominated by thin-bedded (>0.2 m) heterolithic deposits of structureless or planar
331 laminated siltstone, and wavy, ripple and climbing-ripple laminated very-fine grained sandstone
332 (Figs. 14a, b, 15b; Table 2). Rare, debrites are present (Fig. 15b). Lateral lobe fringe deposits
333 experience gradual decrease in sand-content (~50% at the transition of the lobe-off axis to ~20% at
334 transition to distal lobe fringe) and bed thickness (average bed thickness of 0.6 m in lobe off axis to
335 average bed thickness of 0.1 m in lateral lobe fringe). Therefore, pinch-out occurs over several
336 kilometers through thinning and fining of the deposits. In outcrop (e.g. LC4; Fig. 14b), lateral lobe
337 fringes commonly show tabular geometries at the scale of observation (Figs. 14a, b; Table 2). A

338 similar facies transition to a lateral fringe in a lobe was well constrained in the underlying Fan 3 by
339 Prélat et al. (2009, their Lobe 6).

340

341 *Frontal lobe fringe*

342 Figure 12b shows a correlation panel of a single lobe from OC2 to OC5 in LC1 (Fig. 7 and 10). The
343 lobe is identified by abrupt lower and upper contacts to lobe distal fringe deposits. Using the well-
344 constrained paleogeographic map of LC1, this marks the frontal transition from axial lobe deposits
345 (dominated by F1) to a succession marked by hybrid bed deposits, structureless sandstone and
346 siltstone beds. Sandstone deposits show a high degree of amalgamation in OC2, and become
347 progressively less amalgamated down-dip, and increasingly intercalated with thin-bedded siltstone
348 units (Fig. 12b; Fig. 15a). The lobe deposits exhibit a pinch-and-swell geometry (thickening from 2.5
349 m in OC2 to 3.2 m in OC3 and then thinning to 2 m in OC5; Fig. 12b). The sand pinch-out of the lobe
350 occurs abruptly within few hundred meters.

351 Similar facies associations and geometries are observed in the frontal pinch-out of lobe deposits in
352 termination of LC3. The frontal lobe fringe facies association is characterized by dewatered,
353 structureless or planar laminated fine-grained sandstones (Figs. 14c, d, 15a) associated with hybrid
354 beds and rare thick debrites (Table 2). Commonly, the sandstone and hybrid beds of frontal lobe
355 fringes exhibit depositional pinch-and-swell geometries (Fig. 13), which are underlain by siltstones
356 but without any basal truncation. In map view, the pinch-and-swell geometries are mapped as
357 irregular, finger-like bodies aligned with paleoflow (Bouma & Rozmann, 2000; Van der Werff &
358 Johnson, 2003b; Prélat et al., 2009; Hodgson, 2009; Groenenberg et al., 2010). The dimensions of
359 these fingers are 200-300 m in strike width and 1.5 to 2.0 km in dip length. When sand pinch-out
360 occurs overlying sand-prone strata, pronounced fingers do not develop. The percentage of
361 structureless sandstone within the frontal lobe fringe remains high (10 to 50%) up to the point of

362 sandstone pinch-out. Commonly, sandstone pinch-out is abrupt, but thin-bedded siltstones typically
363 continue for several kilometers farther.

364

365

DISCUSSION

366 Lobes do not show simple thinning and fining trends in all directions away from their apex (cf.
367 Groenenberg et al., 2010). Despite showing the widest range of facies, lobe fringes are the least well
368 studied sub-environments of lobes. Lobe fringe complexity has been highlighted by MacPherson
369 (1978) and Pickering (1981; 1983), who demonstrated the significant variability of lobe (or fan)
370 fringe facies. The process reasons behind the observed differences in lateral and frontal lobes
371 fringes, and the subsurface implications of improved identification of fringe setting, are discussed
372 below.

373

Controls on lobe pinch-out geometries

374 Generally, lateral lobe fringe successions are predominantly characterized by deposits from low-
375 density turbidity currents, whereas frontal lobe fringes are dominated by deposits from high-density
376 turbidity currents and other high-concentration flows (structureless sandstones, debrites and hybrid
377 beds; Talling et al., 2012). Lateral lobe fringes fine and thin as they taper away from lobe axis
378 environments (Figs. 12a, 15b). In contrast, basal lobes in the frontal fringes of lobe complexes show
379 abrupt thickness and facies changes (Figs. 12b, 13, 15a). Controls on this distinctive geometry in
380 frontal lobe position could reflect either 1) influence of underlying seabed topography or 2) flow
381 processes and interactions with substrate. Finger-like pinch-outs of frontal lobes are observed within
382 successive lobes of multiple different lobe complexes within the Tanqua depocentre (Bouma &
383 Rozman, 2000; Rozman, 2000; Prélat et al., 2009; Groenenberg et al., 2010). Similar terminations
384 have been observed within other basin-floor lobe systems (Nelson et al., 1992; Twichell et al., 1992),
385 albeit occasionally misinterpreted as channel-forms (e.g. Van der Werff & Johnson, 2003b) due to

386 their elongated shape in planform view and their convex-up form in outcrop. Groenenberg et al.
387 (2010) did not support the presence of pre-existing seabed topography as the main influencing
388 factor because of the common occurrence of finger-like bodies in several basal lobes over several
389 lobe complexes. The repeated formation of seabed relief in a radial finger-like pattern prior to
390 initiation of each lobe complexes, was viewed as unlikely (Groenenberg et al., 2010).

391 Hybrid beds have been reported to be associated with distal lobe settings (Haughton et al., 2003;
392 Talling et al., 2004; Ito, 2008; Hodgson, 2009; Kane and Pontén, 2012; Talling et al., 2012a;
393 Grundvåg et al., 2014; Patacci et al., 2014; Collins et al., 2015; Fonnesu et al., 2015; Southern et al.,
394 2016) and the cohesive nature of the depositing flows is suggested to control the abrupt pinch-out
395 of deposits in this setting (Groenenberg et al., 2010; Kane et al., in review). In frontal lobe fringes,
396 there is evidence that relatively distal turbidity currents eroded and entrained substrate material,
397 preserved as mud-clasts and dispersed mud (Hodgson, 2009, Kane et al., in review). The combined
398 effects of flow deceleration, and increased flow concentration through entrainment, led to
399 enhanced flow stratification and the development of a dense, cohesive basal layer (e.g., McCave and
400 Jones, 1988; Kane & Pontén, 2012; Talling, 2013; Kane et al., in review). The development of a dense
401 basal layer in the flow may have suppressed upward transfer of turbulence resulting in the collapse
402 of the upper part of the flow (McCave & Jones, 1988; Kane et al., in review). The collapse of the
403 upper part of the flow may account for the abrupt pinch-out of both the lower and upper parts of
404 hybrid beds in distal settings, i.e., debritic divisions of hybrid beds rarely out-run the lower cleaner
405 sandstone division. The principal alternative, that turbidity currents fractionated their suspended
406 load and split into forerunning turbidity currents with trailing debris flows (depositing turbidites with
407 linked debrites, Haughton et al., 2003; Haughton et al., 2009), may account for thicker debrites, that
408 are observed to be deposited within the finger-like structures (see Fig. 13c). These may have over-
409 run, or taken a different course, to their forerunning turbidity currents. Deposits of high-density
410 turbidity currents are able to create their own pathways and become successively more elongated
411 down-dip, forming finger-like bodies. These finger-like structures of frontal lobes are connected by

412 thin-beds creating a webbed bird's foot geometry in planform (Fig. 13, 16a). This accords with results
413 by Groenenberg et al. (2010) from process-based numerical modelling of lobes, who suggested that
414 depositional relief of preceding lobes could help to focus these types of flow into distal areas.
415 Elongated beds have been produced experimentally by Luthi (1981) showing that velocity of the
416 turbidity currents was highest along the central axis. The frontal pinch-out of lobe complexes is
417 accompanied by abrupt thickness decrease and occurs over a few hundred meters (Fig. 15a).

418 The lateral fringe of a lobe forms a wedge-like geometry that thins away from the lobe axis and off-
419 axis (Fig. 15b) as deposits fine gradually over a few kilometers (Fig. 16a). Lateral lobe fringe deposits
420 dominantly record the accumulated products of low-density turbidity currents. Luthi's (1981)
421 experiments show that flow velocities are lowest in these flow marginal areas, and the flow
422 thickness decrease is greatest laterally away from the central flow axis. Depositional relief of
423 preceding lobe deposits probably had a relatively minor influence on low-density flows, as these can
424 surmount seabed topography (e.g., Brunt et al., 2004; Bakke et al., 2013). Their run-out distance is
425 therefore primarily dependent on their thickness and volume (Wynn et al., 2002). The deposits of
426 the low-density turbidity currents probably form laterally extensive radial deposits which are higher
427 in proportion at the lateral fringe, owing to the forward momentum and lack of lateral spreading of
428 the higher concentration flows in the axial areas. In the frontal fringe setting, the low-density
429 turbidity currents, for the most-part, out ran the flows responsible for depositing the hybrid beds to
430 deposit in distal fringe settings. Thin stand-alone debrites recorded in the lateral fringes deposits are
431 inferred to have been deposited by debris flows which bypassed the majority of the lobe to be
432 deposited in its fringe (Talling et al., 2012b; Ducassou et al., 2013).

433

434 *Role of confinement*

435 The difference in lateral and frontal lobe fringe within LC1 and LC3 has been documented in a
436 relatively unconfined basin-floor setting. In basins where lobes do not feel basin confinement,
437 compensational stacking will result in alternating successions of lobe axis and off-axis environments,
438 with lobe fringe and distal fringe environments (Prélat and Hodgson 2013). Therefore, it is possible
439 that frontal and lateral lobe fringes will be present in a 1-D section (e.g. core) through a single lobe
440 complex. Flow confinement has been documented to be an important autogenic factor in the
441 control of dispersal patterns and lobe stacking patterns (e.g. Piper & Normark, 1983; Smith &
442 Joseph, 2004; Amy et al., 2004, Twichell et al., 2005; Macdonald et al., 2011; Marini et al., 2011;
443 Southern et al., 2015; Marini et al., 2015).

444 With increased seabed confinement, lobes will be forced stack aggradationally or longitudinally
445 rather than compensationally. This would lead to a clearer segregation of frontal and lateral lobe
446 fringes. Even subtle intrabasinal slopes, with angles as small as a fraction of a degree, have been
447 shown to modify stacking patterns and facies distribution considerably. Sychala et al. (2016) show
448 that an intrabasinal slope ($< 0.5^\circ$) in the Laingsburg depocentre, Karoo Basin, led to aggradational
449 stacking of lateral lobe fringes in multiple stacked lateral lobe complex fringes, compared to
450 compensational stacking patterns in the unconfined part of the basin. The aggradation of multiple
451 lateral lobe fringes in LC1 (Fig. 11), allied to the persistent thinning and paleocurrent trends (Fig. 10)
452 could be used to infer the presence of a subtle confining N-S oriented slope. The lateral lobe fringe
453 facies association reflects the overall aggradational trend with sedimentary features such as climbing
454 bedforms and predominant climbing-ripple lamination. Similar observations have been made from
455 the Silurian sand-prone deep-water systems of the Welsh Basin (cf. Smith 1987a,b; Wilson et al.,
456 1992; Smith 2004). It is not clear if there are distinctive lateral or frontal facies trends in more highly
457 confined basin settings; this is an area that warrants further investigation.

458 *Subsurface implications*

459 The documented differences in sedimentology and architecture of lateral and frontal lobe fringes
460 have several implications for subsurface applications. Facies recognition criteria established in this
461 study can help determine internal division of lobe complexes in 1D datasets, e.g. core data, to help
462 improve paleogeographic reconstructions. Stacking of lobe fringe types could be used as an indicator
463 of the degree and orientation of seabed topography. In an unconfined setting, vertical stacking of
464 frontal and lateral lobe fringes in a lobe complex are possible, whereas in settings influenced by
465 relief stacked successions of frontal lobe fringes (hybrid bed-rich deposits) or lateral lobe fringes
466 (thin-bedded heterolithic deposits) in a lobe complex can accumulate.

467 Lobe fringe deposits form heterogeneities within deep-water fan deposits (e.g. Etienne et al., 2012;
468 Collins et al., 2015; Grecula et al., 2015). Generally, frontal lobe fringes have higher sandstone
469 percentages (~50%). However, the high proportion of hybrid beds means that permeability values
470 are likely to be considerably lower than within structureless and structured sandstones. This
471 conforms to the conclusions of Marchand et al. (2015) who observed that the presence of silt-sized
472 particles and ductile, platy shaped grains in distal sand-rich successions decreases reservoir quality;
473 furthermore, Porten et al. (2016) demonstrate that for a given porosity, hybrid beds may have
474 permeabilities one or two order of magnitude lower than turbidites. Thick-bedded deposits can be
475 expected in frontal lobe fringes, but amalgamation is rare. Lateral fringe deposits gradually decrease
476 in sand-content (~50% at transition structured sandstones of the lobe-off axis to ~20% at transition
477 to distal lobe fringe) and bed thickness. Bed amalgamation is not observed. Permeability and
478 porosity values are expected to be relatively low, and decrease gradually as the deposits thin and
479 fine. Lobe fringes have the potential to be stratigraphic traps (*sensu* Levorsen, 1936) with their
480 confining element being lateral depositional changes especially at the margins of a lobe complex
481 that are encased by hemipelagic deposits. Lateral lobe fringes are dominated by lateral gradation of
482 sandstone to silty mudstone with widespread waste zones (cf. Rittenhouse, 1972; Biddle and
483 Wielchowsky, 1994). Frontal lobe fringes, however, are characterized by their abrupt pinch-out style
484 (cf. Rittenhouse, 1972; Biddle and Wielchowsky, 1994) and are connected to the high-quality

485 reservoir sandstones of the lobe axis and lobe off-axis up-dip. Therefore, frontal fringes are
486 considered to have greater potential as viable stratigraphic trap targets.

487 **CONCLUSIONS**

488 Lobe fringe successions are the least well studied sub-environments of submarine lobe deposits
489 despite showing the widest range of facies and being critical to many lobe stratigraphic trap targets.
490 An integrated outcrop and research borehole data set uses thickness and grain-size trends, facies
491 distribution and depositional geometries, to constrain two distinctive lobe fringe settings; frontal
492 lobe fringe and lateral lobe fringe. Frontal lobe fringes are characterized by structureless sandstone
493 and hybrid bed deposits. They can exhibit elongated finger-like shapes with abrupt sandstone pinch-
494 out. Lateral fringes are dominated by heterolithic traction-influenced deposits that gradually thin
495 and fine to form a simple taper. Therefore, lobes do not show simple thinning and fining trends in all
496 directions away from their apex.

497 The dominant flow processes control the differences in facies associations and geometries of the
498 two lobe fringe sub-environments. Frontal lobe fringes are characterized by deposits of the highest
499 energy parts of turbidity currents that passed through the axis of the lobe, and maintained the
500 highest momentum. In contrast, lateral fringes are dominated by deposits from low-density turbidity
501 currents that are prone to tractional reworking. Distinguishing frontal and lateral lobe fringes
502 improves prediction of facies distributions, and their stacking patterns, and can help to build more
503 accurate reconstructions of lobe complexes, even without well-exposed outcrops arranged in 3-D
504 distributions. Compensational stacking of lobes in unconfined settings can lead to stratigraphic
505 alternations of frontal and lateral lobe fringes in lobe complexes, whereas it is speculated that in
506 confined settings aggradational to longitudinal stacking of frontal and lateral fringes will result in
507 stronger stratigraphic and geographic segregation. The development of recognition criteria to
508 distinguish between frontal and lateral lobe fringes will help to support paleogeographic
509 reconstructions, and inform the appraisal of stratigraphic trap prospects in the subsurface.

510

511

ACKNOWLEDGEMENTS

512 The authors would like to thank the local farmers of the Tanqua region of South Africa for
513 permission to carry out field studies on their land. Further, we would like to thank Aurelia Privat for
514 field assistance. The LOBE 2 consortium project of which this research forms a part is supported by
515 sponsorship from Anadarko, Bayerngas Norge, BG Group, BHPBilliton, BP, Chevron, DONG Energy,
516 ENGIE, Maersk, Marathon, Petrobras, Premier Oil, Shell, Statoil, Total, VNG Norge and Woodside, for
517 which the authors are grateful. Reviews by the Journal of Sedimentary Research Associate Editor
518 Morgan Sullivan and reviewers Zoltan Sylvester and Sten-Andreas Grundvåg greatly improved the
519 manuscript.

520

REFERENCES

521 Allen, J.R.L., 1971, Instantaneous sediment deposition rates deduced from climbing-ripple cross-
522 lamination: Journal of Geological Society London, v. 127, p. 553-561.

523

524 Allen, J.R.L., 1973, A classification of climbing-ripple cross-lamination: Journal of the Geological
525 Society London, v. 129, p. 537–541.

526

527 Allen, J.R.L., 1982, Sedimentary Structures: Their Character and Physical Basis vol. 1,2: Elsevier,
528 Amsterdam (593pp., 663 pp.)

529

530 Amy, L.A., McCaffrey, W.D. and Kneller, B.C., 2004, The influence of a lateral basin-slope on the
531 depositional patterns of natural and experimental turbidity currents, *in* Joseph, P. and Lomas, S.A,
532 eds., Deep-Water Sedimentation in the Alpine Basin of Se France: New Perspectives on the Gres
533 d'Annot and related systems: Geological Society London Special Publication, v. 221, p. 311-330.

534

535 Arnott, R.W.C., and Hand, B.C., 1989, Bedforms, Primary Structures and Grain Fabric in the Presence
536 of Suspended Sediment Rain: *Journal of Sedimentary Petrology*, v. 59, p. 1062-1069.

537

538 Bakke, K., Kane, I.A., Martinsen, O.J., Petersen, S.A., Johansen, T.A., Hustoft, S., Jacobsen, F.H., and
539 Groth, A., 2013, Seismic modeling in the analysis of deep-water sandstone termination style: *AAPG*
540 *Bulletin*, v. 97, p. 1395- 1419.

541

542 Best, J., and Bridge, J., 1992, The morphology and dynamics of low amplitude bedwaves upon upper
543 stage plane beds and the preservation of planar laminae: *Sedimentology*, v. 39, p. 737-752.

544

545 Biddle, K.T., and Wielchowsky, C.C., 1994, Hydrocarbon traps: *AAPG Memoir*, v. 60, p. 219-235.

546

547 Bouma, A.H., 1962, *Sedimentology of some flysch deposits: a graphic approach to facies*
548 *interpretation*. Elsevier, Amsterdam/New York, 168pp.

549

550 Bouma, A.H., 2000, Fine-Grained, Mud-Rich Turbidite Systems: Model and Comparison with Coarse-
551 Grained, Sand-Rich Systems, *in* Bouma, A.H., and Stone, C.G., eds., *Fine-grained Turbidite Systems* ,
552 *AAPG Memoir 72/SEPM Special Publication*, v. 68, p. 9-19.

553

554 Bouma, A.H., and Wickens, H.d.V., 1991, Permian passive margin submarine fan complex, Karoo
555 Basin, South Africa: possible model to Gulf of Mexico: *Gulf Coast Association of Geological Societies*,
556 v. 41, p. 30-42.

557

558 Bouma, A.H., and Rozman, D.J., 2000, Characteristics of fine grained outer fan fringe turbidite
559 systems, *in* Bouma, A.H., and Stone, C.G., eds., *Fine-grained Turbidite Systems*, AAPG Memoir
560 72/SEPM Special Publication, v. 68, p. 291–298.

561

562 Brunt, R.L., McCaffrey, W.D., and Kneller, B.C., 2004, Experimental modeling of the spatial
563 distribution of grain size developed in a fill-and-spill mini-basin setting: *Journal of Sedimentary*
564 *Research*, v. 74, p. 438-446.

565

566 Catuneanu, O., Hancox, P.J., and Rubridge, B.S., 1998, Reciprocal flexural behaviour and contrasting
567 stratigraphies: a new basin development model for the Karoo retroarc foreland system, South Africa:
568 *Basin Research*, v. 10, p. 417-439.

569

570 Collins, J., Kenyon-Roberts, S., Cullen, B., White, J., Bordas-Le Floch, N., and Downey, J., 2015, Arran
571 Field: a complex heterolithic reservoir on the margins of the Forties Fan System, *in* McKie, T., Rose,
572 P.T.S., Hartley, A.J., Jones, D.W. and Armstrong, T.L., eds., *Tertiary Deep-Marine Reservoirs of the*
573 *North Sea Region: Geological Society London Special Publication*, v. 403, p. 185-217.

574

575 Davis, C., Haughton, P., McCaffrey, W., Scott, E. Hogg, N., and Kitching, D., 2009, Character and
576 distribution of hybrid sediment gravity flow deposits from the outer Forties Fan, Paleocene Central
577 North Sea, UKCS: *Marine and Petroleum Geology*, v. 26, p. 1919-1939.

578

579 Deptuck, M.E., Piper, D.J.W., Savoye, B., and Gervais, A., 2008, Dimensions and architecture of late
580 Pleistocene submarine lobes off the northern margin of East Corsica: *Sedimentology*, v. 55, p. 869–
581 898.

582

583 Ducassou, E., Migeon, S., Capotondi, L., and Mascle, J., 2013, Run-out distance and erosion of debris-
584 flows in the Nile deep-sea fan system: Evidence from lithofacies and micropaleontological analyses:
585 Marine and Petroleum Geology, v. 38, p. 102-123.

586

587 Dudley, P.R.C., Rehmer, D.E., and Bouma, A.H., 2000, Reservoir-Scale Characteristics of Fine-Grained
588 Sheet Sandstone, Tanqua Karoo Subbasin, South Africa: GCSSEPM Foundation 20th Annual Research
589 Conference. Deep-Water Reservoirs of the World, December 3-6, 200x.

590

591 Etienne, S., Mulder, T., Bez, M., Desaubliaux, G., Kwasniewski, A., Parize, O., Dujoncquoy, E., and
592 Salles, T., 2012, Multiple scale characterization of sand-rich distal lobe deposit variability: Examples
593 from the Annot Sandstones Formation, Eocene–Oligocene, SE France: Sedimentary Geology, v. 273-
594 274, p. 1-18.

595

596 Flint, S.S., Hodgson, D.M., Sprague, A.R., Brunt, R.L., van der Merwe, W.C., Figueiredo, J., Prélat, A.,
597 Box, D., Di Celma, C., and Kavanagh, J.P., 2011, Depositional architecture and sequence stratigraphy
598 of the Karoo basin floor to shelf edge succession, Laingsburg depocentre, South Africa: Marine and
599 Petroleum Geology, v. 28, p. 658-674.

600

601 Fonnesu, M., Haughton, P., Felletti, F., and McCaffrey, W., 2015, Short length-scale variability of
602 hybrid event beds and its applied significance: Marine and Petroleum Geology, v. 67, p. 583-603.

603

604 Gervais, A., Savoye, B., Mulder, T., and Gonthier, E., 2006, Sandy modern turbidite lobes: A new
605 insight from high resolution seismic data: Marine and Petroleum Geology, v. 23, p. 485-502.

606

607 Goldhammer, R.K., Wickens, D.H., Bouma, A.H., and Wach, G., 2000, Sequence Stratigraphic
608 Architecture of the Late Permian Tanqua Submarine Fan Complex, Karoo Basin, South Africa, , *in*

609 Bouma, A.H., and Stone, C.G., eds., *Fine-grained Turbidite Systems* , AAPG Memoir 72/SEPM Special
610 Publication, v. 68, p. 165-172.
611

612 Grecula, M., Hognestad, J., Price, S., Boya Ferrero, M., De Bruijn, G., Noraberg, K.T., Engenes, K.,
613 Mears, P., Van Ojik, K., and McGarva, R., 2015, Interplay of fan-fringe reservoir deterioration and
614 hydrodynamic aquifer: understanding the margins of gas development in the Ormen Lange Field, *in*
615 McKie, T., Rose, P.T.S., Hartley, A.J., Jones, D.W., and Armstrong, T.L., eds., *Tertiary Deep-Marine*
616 *Reservoirs of the North Sea Region: Geological Society London Special Publication*, v. 403, p.157-183.
617

618 Groenenberg, R.M., Hodgson, D.M., Pr lat, A., Luthi, S.M., and Flint, S.S., 2010, Flow-Deposit
619 Interaction in Submarine Lobes: Insights from Outcrop Observations and Realizations of the Process-
620 Based Numerical Model: *Journal of Sedimentary Research*, v. 80, p. 252-267.
621

622 Grundv g, S.A., Johannessen, E.P., Helland-Hansen, W., and Plink-Bj rklund, P., 2014, Depositional
623 architecture and evolution of progradationally stacked lobe complexes in the Eocene Central Basin
624 of Spitsbergen: *Sedimentology*, v. 61, p. 535-569.
625

626 Haughton, P.D.W., Barker, S.P., and McCaffrey, W.D., 2003, 'Linked' debrites in sand-rich turbidite
627 systems – Origin and significance: *Sedimentology*, v. 50, p. 459-482.
628

629 Haughton, P., Davis, C., McCaffrey, W., and Barker, S., 2009, Hybrid sediment gravity flow deposits –
630 Classification, origin and significance: *Marine and Petroleum Geology*, v. 26, p. 1900-1918.
631

632 Hodgson, D.M., Flint, S.S., Hodgetts, D., Drinkwater, N.J., Johannessen, E.P., and Luthi, S., 2006,
633 Stratigraphic evolution of fine-grained submarine fan systems, Tanqua depocentre, Karoo Basin,
634 South Africa: *Journal of Sedimentary Research*, v. 76, p. 20– 40.

635

636 Hodgson, D.M., 2009, Distribution and origin of hybrids beds in sand-rich submarine fans of the
637 Tanqua depocentre, Karoo Basin, South Africa: *Marine and Petroleum Geology*, v. 26, p. 1940-1956.

638

639 Hodgson, D.M., Kane, I.A., Flint, S.S., Brunt, R.L. and Ortiz-Karpf, A., 2016, Time-Transgressive
640 Confinement On the Slope and the Progradation of Basin-Floor Fans: Implications For the Sequence
641 Stratigraphy of Deep-Water Deposits: *Journal of Sedimentary Research*, v. 86, p.73-86.

642 Hofstra, M., Hodgson, D.M., Peakall, J., and Flint, S.S., 2015, Giant-scour fills in ancient channel-lobe
643 transition zones: Formative processes and depositional architecture: *Sedimentary Geology*, v. 329, p.
644 98-114.

645

646 Hunter, R.E., 1977, Terminology of cross-stratified sedimentary layers and climbing-ripple structures:
647 *Journal of Sedimentary Research*, v. 47, p. 697–706.

648

649 Ito, M., 2008, Downfan Transformation from Turbidity currents to debris flows at a Channel-to-Lobe
650 Transitional Zone: The Lower Pleistocene Otadai Formation, Boso Peninsula, Japan: *Journal of*
651 *Sedimentary Research*, v. 78, p. 668-682.

652

653 Iverson, R.M., 1997, The physics of debris flow: *Reviews of Geophysics*, v. 35, p. 245-296.

654

655 Jegou, I., Savoye, B., Pirmez, C., and Droz, L., 2008, Channel-mouth lobe complex of the recent
656 Amazon fan: The missing piece: *Marine Geology*, v. 252, p. 62–77.

657

658 Jobe, Z.R., Lowe, D.R., Morris, W.R., 2012, Climbing-ripple successions in turbidite systems:
659 depositional environments, sedimentation rates and accumulation times: *Sedimentology*, v. 59, p.
660 867-898.

661

662 Johnson, S.D., Flint, S.S., Hinds, D., and Wickens, H.d.V., 2001, Anatomy of basin floor to slope
663 turbidite systems, Tanqua Karoo, South Africa: sedimentology, sequence stratigraphy and
664 implications for subsurface prediction: *Sedimentology*, v. 48, p. 987–1023.

665

666 Jopling, A.V., and Walker, R.G., 1968, Morphology and origin of ripple-drift cross-lamination, with
667 examples from the Pleistocene of Massachusetts: *Journal of Sedimentary Research*, v. 38, p. 971–
668 984.

669

670 Kane, I.A. and Pontén, A.S.M., 2012, Submarine transitional flow deposits in the Paleogene Gulf of
671 Mexico: *Geology*, v. 40, p. 1119-1122.

672 Kane, I., Pontén, A., Vangdal, B., Eggenhuisen, J., Hodgson, D.M. and Spychala, Y.T., in review, The
673 stratigraphic record and processes of turbidity current transformation across deep-marine lobes:
674 *Sedimentology*.

675

676 Kneller, B.C., and Branney, M.J., 1995, Sustained high-density turbidity currents and the deposition
677 of thick massive sands: *Sedimentology*, v. 42, p. 607-616.

678

679 Leclair, S.F., and Arnott, R.W.C., 2005, Parallel Lamination Formed by High-Density Turbidity
680 Currents: *Journal of Sedimentary Research*, v. 75, p. 1-5.

681

682 Levorsen, A.I., 1936, Structural versus structural accumulation: *AAPG Bulletin*, v. 20, p. 521-530.

683

684 Lowe, D.R., 1982, Sediment gravity flows: II. Depositional models with special reference to the
685 deposits of high-density turbidity currents: *Journal of Sedimentary Petrology*, v. 52, p. 279-297.

686

687 Lowe, D.R., and Guy, M., 2000, Slurry-flow deposits in the Britannia Formation (Lower Cretaceous),
688 North Sea: a new perspective on the turbidity current and debris flow problem: *Sedimentology*, v.
689 47, p. 31-70.
690

691 Luthi, S., 1981, Experiments on non-channelized turbidity currents and their deposits: *Marine*
692 *Geology*, v. 40, M59-M68.
693

694 Luthi, S.M., Hodgson, D.M., Geel, C.R., Flint, S.S., Goedbloed, J.W., Drinkwater, N.J., and
695 Johannessen, E.P., 2006, Contribution of research borehole data to modelling fine-grained turbidite
696 reservoir analogues, Permian Tanqua-Karoo basin-floor fans (South Africa): *Petroleum Geosciences*,
697 v.12, p. 175-190.
698

699 Macdonald, H.A., Peakall, J., Wignall, P.B., and Best, J., 2011, Sedimentation in deep-sea lobe
700 elements: implications for the origin of the thickening-upward sequences: *Journal of the Geological*
701 *Society London*, v. 168, p. 319-331.
702

703 MacPherson, B.A., 1978, Sedimentation and Trapping Mechanism in Upper Miocene Stevens and
704 Older Turbidite Fans of Southeastern San Joaquin Valley, California: *AAPG Bulletin*, v. 62, p. 2243-
705 2274.
706

707 Marchand, A.M.E., Apps, G., Li, W., and Rotzien, J.R., 2015, Depositional processes and impact on
708 reservoir quality in deepwater Paleogene reservoirs, US Gulf of Mexico: *AAPG Bulletin*, v. 99, p.
709 1635-1648.
710

711 Marini, M., Milli, S., and Moscatelli, M., 2011, Facies and architecture of the Lower Messinian
712 turbidite complexes from the Laga Basin (central Apennines, Italy): *Journal of Mediterranean Earth*
713 *Science*, v. 3, p. 45-72.

714 Marini, M., Salvatore, M., Ravnås, R., and Moscatelli, M., 2015, A comparative study of confined vs.
715 semi-confined turbidite lobes from the Lower Messinian Laga Basin (Central Apennines, Italy):
716 Implications for assessment of reservoir architecture: *Marine and Petroleum Geology*, v. 63, p. 142-
717 165.

718

719 Masalimova, L.U., Lowe, D.R., Sharman, G.R., King, P.R., and Arnot, M.J., 2016, Outcrop
720 characterization of a submarine channel-lobe complex: The Lower Mount Messenger Formation,
721 Taranaki Basin, New Zealand: *Marine and Petroleum Geology*, v. 71, p.360-390.

722

723 McCave, I.N., and Jones, K.P.N., 1988, Deposition of ungraded muds from high-density non-turbulent
724 turbidity currents: *Nature*, v. 333, p. 250-252.

725

726 Morris, W.R., Scheilhing, M.H., Wickens, DeV., Bouma, A.H., 2000, Reservoir architecture of
727 deepwater sandstones: examples from the Skoorsteenberg Formation, Tanqua Karoo Sub-Basin,
728 South Africa, *in* Weimer, P., Slatt, R.M., Bouma, A.H., and Lawrence, D.T., eds., *Deep-water reservoirs*
729 *of the world: Gulf Coast Section SEPM Foundation, Twentieth Annual Research Conference*, p. 1010-
730 1032.

731

732 Mutti, E., 1977, Distinctive thin-bedded turbidite facies and related depositional environments in the
733 Eocene Hecho Group (South-central Pyrenees, Spain): *Sedimentology*, v. 24, p. 107-131.

734

735 Mutti, E., 1992, *Turbidite Sandstones*. Instituto di Geologia, Università di Parma & AGIP, San Donato
736 Milanese, Italy, 275pp.

737

738 Nagatomo, A., and Archer, S., 2015, Termination geometries and reservoir properties of the Forties
739 Sandstone pinch-out, East Central Graben, UK North Sea, *in* McKie, T., Rose, P.T.S., Hartley, A.J.,
740 Jones, D.W., and Armstrong, T.L., eds., Tertiary Deep-Marine Reservoirs of the North Sea Region:
741 Geological Society London Special Publication, v. 403, p. 133-155.

742

743 Nelson, C.H., Twichell, D.C., Schwab, W.C., Lee, H.J., and Kenyon, N.H., 1992, Upper Pleistocene
744 turbidite sand beds and chaotic silt beds in the channelized, distal, outer-fan lobes of the Mississippi
745 fan: *Geology*, v. 20, p. 693–696.

746

747 Normark, W.R., 1978, Fan Valleys, Channels, and Depositional Lobes on Modern Submarine Fans:
748 Characters for Recognition of Sandy Turbidite Environments: *AAPG Bulletin*, v. 62, p. 912-931.

749

750 Patacci, M., Haughton, P.D.W., and McCaffrey, W.D., 2014, Rheological complexity in sediment
751 gravity flows forced to decelerate against a confining slope, Braux, SE France: *Journal of Sedimentary*
752 *Research*, v. 84, p. 270-277.

753

754 Pickering, K. T., 1981, Two types of outer fan lobe sequence, from the late Precambrian Kongsfjord
755 Formation submarine fan, Finnmark, North Norway: *Journal of Sedimentary Research*, v. 51, p. 1277-
756 1286.

757

758 Pickering, K. T., 1983, Transitional submarine fan deposits from the late Precambrian Kongsfjord
759 Formation submarine fan, NE Finnmark, N. Norway: *Sedimentology*, v. 30, 181-199.

760

761 Piper, D.J.W., and Normark, W.R., 1983, Turbidite depositional patterns and flow characteristics,
762 Navy Submarine Fan, California Borderland: *Sedimentology*, v. 30, p. 681-694.

763

764 Porten, K.W., Kane, I.A., Warchoř, M.J. and Southern, S.J., in press. A sedimentological process-based
765 approach to depositional reservoir quality of deep-marine sandstones: an example from the Springar
766 Formation, north-western Vřoring Basin, Norwegian Sea. *Journal of Sedimentary Research*.

767

768 Prřelat, A., Hodgson, D.M., and Flint, S.S., 2009, Evolution, architecture and hierarchy of distributary
769 deep-water deposits: a high-resolution outcrop investigation from the Permian Karoo Basin, South
770 Africa: *Sedimentology*, v. 56, p. 2132-2154.

771

772 Prřelat, A., Covault, J.A., Hodgson, D.M., Fildani, A., and Flint S.S., 2010, Intrinsic controls on the range
773 of volumes, morphologies, and dimensions of submarine lobes: *Sedimentary Geology*, v. 232, p. 66-
774 76.

775

776 Prřelat, A., and Hodgson, D.M., 2013, The full range of turbidite bed thickness patterns in submarine
777 lobes: controls and implications: *Journal of the Geological Society London*, v. 170, p. 1-6.

778

779 Pysklywec, R.N., and Mitrovica, J.X., 1999, The role of subduction-induced subsidence in the
780 evolution of the Karoo Basin: *The Journal of Geology*, v. 107, p. 155-164.

781

782 Rittenhouse, G., 1972, Stratigraphic-Trap Classification: *Geologic Exploration Methods*, in Gould,
783 H.R., ed., *Stratigraphic Oil and Gas Fields—Classification, Exploration Methods, and Case Studies*:
784 AAPG Memoir, v. 16, p. 14-28.

785

786 Rozman, D.J., 2000, Characterization of a Fine-Grained Outer Submarine Fan Deposit, Tanqua-Karoo
787 Basin, South Africa , in Bouma, A.H., and Stone, C.G., eds., *Fine-grained Turbidite Systems*: AAPG
788 Memoir 72/SEPM Special Publication, v. 68, p. 279-290.

789

790 Saller, A., Werner, K., Sugiawan, F., Cebastian, A., May, R., Glenn, D., and Barker, C., 2008,
791 Characteristics of Pleistocene deep-water fan lobes and their application to an upper Miocene
792 reservoir model, offshore East Kalimantan, Indonesia: AAPG Bulletin, v. 92, p. 919–949.

793

794 Smith, R., 1987a, Structure and deformation history of the Central Wales Synclinorium, northeast
795 Dyfed: evidence for a long-lived basement structure: Geological Journal, v. 22, p.183-198.

796

797 Smith, R., 1987b, The *Griestoniensis* Zone Turbidite System, Welsh Basin, in Leggett, J.K. and Zuffa,
798 C.G., eds., Marine Clastic Sedimentology: Concepts and Case Studies: Graham & Trotman, London, p.
799 89-107.

800

801 Smith, R., 2004, Turbidite systems influenced by structurally induced topography in the multi-
802 sourced Welsh Basin, in Lomas, S.A. and Joseph, P., eds., Confined Turbidite Systems: Geological
803 Society London Special Publication, v. 222, p. 209-228.

804

805 Smith, R., and Joseph, P., 2004, Onlap stratal architectures in the Gres d'Annot: geometric models
806 and controlling factors, in Joseph, P. and Lomas, S.A., eds., Deep-Water Sedimentation in the Alpine
807 Basin of Se France: New Perspectives on the Gres d'Annot and related systems: Geological Society
808 London Special Publication, v. 221, p. 389-399.

809

810 Sømme, T.O., Helland-Hansen, W., Martinsen, O., and Thurmond, J.B., 2009, Relationships between
811 morphological and sedimentological parameters in source-to-sink systems: a basis for predicting
812 semi-quantitative characteristics in subsurface systems: Basin Research, v. 21, p. 361–387.

813

814 Southard, J.B., 1991, Experimental determination of bed-form stability: Annual Review of Earth and
815 Planetary Science, v. 19, p. 423-455.
816

817 Southern, S.J., Patacci, M., Felletti, F., and McCaffrey, W.D., 2015, Influence of flow containment and
818 substrate entrainment upon sandy hybrid event beds containing a co-genetic mud-clast rich division:
819 Sedimentary Geology, v. 321, p. 105-122.
820

821 Southern, S.J., Kane, I.A., Warchoř, M.J., Porten, K.W. and McCaffrey, W.D., 2016. Hybrid event beds
822 dominated by transitional-flow facies: Character, distribution and significance in the Maastrichtian
823 Springar Formation, north-west Vřoring Basin, Norwegian Sea. Sedimentology, published online. DOI:
824 10.1111/sed.12323

825 Spychala, Y.T., Hodgson, D.M., Flint, S.S., and Mountney, N.P., 2015, Constraining the sedimentology
826 and stratigraphy of submarine intraslope lobe deposits using exhumed examples from the Karoo
827 Basin, South Africa: Sedimentary Geology, v. 322, p. 67-81.
828

829 Spychala, Y.T., Hodgson, D.M., Stevenson, C.J., and Flint, S.S., 2016, Aggradational lobe fringes: the
830 influence of subtle intrabasinal topography on sediment gravity flow processes and lobe stacking
831 patterns: Sedimentology, published online. DOI: 10.1111/sed.12315
832

833 Talling, P.J., Amy, L.A., Wynn, R.B., Peakall, J., and Robinson, M., 2004, Beds comprising debrite
834 sandwiched within co-genetic turbidite: origin and widespread occurrence in distal depositional
835 environments: Sedimentology, v. 51, p. 163-194.
836

837 Talling, P.J., Masson, D.G., Sumner, E.J., and Malgesini, G., 2012a, Subaqueous sediment density
838 flows: Depositional processes and deposit types: Sedimentology, v. 59, p. 1937-2003.
839

840 Talling, P.J., Malgesini, G., Sumner, E.J., Amy, L.A., Felletti, F., Blackbourn, G., Nutt, C., Wilcox, C.,
841 Harding, I.C., and Akbari, S., 2012b, Planform geometry, stacking pattern, and extrabasinal origin of
842 low strength and intermediate strength cohesive debris flow deposits in the Marnoso-arenacea
843 Formation, Italy: *Geosphere*, v. 8, p. 1207-1230.

844

845 Talling, P.J., 2013, Hybrid submarine flows comprising turbidity current and cohesive debris flow:
846 Deposits, theoretical and experimental analyses, and generalized models: *Geosphere*, v. 9, p. 460-
847 488.

848

849 Tankard, A., Welsink, H., Aukes, P., Newton, R., and Stettler, E., 2009, Tectonic evolution of the Cape
850 and Karoo basins of South Africa: *Marine and Petroleum Geology*, v. 26, p. 1379-1412.

851

852 Twichell, D.C., Schwab, W.C., Nelson, C.H., Kenyon, N.H., and Lee, H.J., 1992, Characteristics of a
853 sandy depositional lobe on the outer Mississippi fan from DeaMARC IA sidescan sonar images:
854 *Geology*, v. 20, p. 689–692.

855

856 Twichell, D.C., Cross, V.A., Hanson, A.D., Buck, B.J., Zybala, J.G., and Rudin, M.J., 2005, Seismic
857 architecture and lithofacies of turbidites in Lake Mead (Arizona and Nevada, U.S.A.), an analogue for
858 topographic complex basins: *Journal of Sedimentary Research*, v. 75, p. 134-148.

859

860 van der Werff, W., and Johnson, S., 2003a, High resolution stratigraphic analysis of a turbidite
861 system, Tanqua Karoo Basin, South Africa: *Marine and Petroleum, Geology*, v. 20, p. 45-69.

862

863 van der Werff, W., and Johnson, S., 2003b, Deep-sea fan pinch-out geometries and their relationship
864 to fan architecture, Tanqua Karoo basin (South Africa): *Geologische Rundschau*, v. 92, p. 728-742.

865

866 Visser, J.N.J., 1997, Deglaciation sequences in the Permo-Carboniferous Karoo and Kalahari basins of
867 the southern Africa: a tool in the analysis of cyclic glaciomarine basin fills: *Sedimentology*, v. 44, p.
868 507-521.

869

870 Visser, J.N.J, and Prackelt, H.E., 1996, Subduction, mega-shear systems and Late Palaeozoic basin
871 development in the African segment of Gondwana: *Geologische Rundschau*, v. 85, p. 632-646.

872

873 Wickens, H.d.V., 1994, Basin floor fan building turbidites of the southwestern Karoo Basin, Permian
874 Ecca Group. PhD Thesis, Port Elizabeth University, South Africa, 233pp.

875

876 Wickens, H.d.V., and Bouma, A.H., 2000, The Tanqua Fan Complex, Karoo Basin, South Africa –
877 outcrop analogue for fine-grained, deepwater deposits, *in* Bouma, A.H., and Stone, C.G., eds., *Fine-*
878 *grained Turbidite Systems* , AAPG Memoir 72/SEPM Special Publication, v. 68, p. 153–165.

879

880 Wild, R.J., Hodgson, D.M., and Flint, S.S., 2005, Architecture and stratigraphic evolution of multiple,
881 vertically-stacked slope-channel complexes, Tanqua depocentre, Karoo Basin, South Africa, *in*
882 Hodgson, D.M., and Flint, S.S., eds., *Submarine Slope Systems, Processes and Products: Geological*
883 *Society London Special Publication*, v. 244, p. 89–112.

884

885 Wild, R., Flint, S.S., and Hodgson, D.M., 2009, Stratigraphic evolution of the upper slope and the shelf
886 edge in the Karoo Basin, South Africa. *Basin Research*, v. 21, p. 502-527.

887

888 Wilson, D., Davies, J.R., Waters, R.A., and Zalasiewicz, J.A., 1992, A fault-controlled depositional
889 model for the Aberystwyth Grits turbiditic system: *Geological Magazine*, 129, p. 595-607.

890

891 Wynn, R.B., Weaver, P.E., Masson, D.G., and Stow, D.A.V., 2002, Turbidite depositional architecture
892 across three interconnected deep-water basins on the north-west African margin: *Sedimentology*, v.
893 49, p. 669-695.

894

895 **Figure Captions**

896 Fig. 1: A: Simplified model indicating the different sub-environments in a lobe (redrawn from Prélat
897 et al., 2009). B: Plan-form view of five-fold lobe hierarchy: bed to bed set, lobe element, lobe, lobe
898 complex and lobe complex set (modified from Prélat et al., 2010).

899 Fig. 2: A: The Tanqua depocentre inboard of the Cape Fold Belt (Cederberg and Swartberg branches).
900 The square indicates the location of the study area. B: Stratigraphy of the Tanqua depocenter
901 (redrawn after Wild et al., 2009). The Skoorsteen Formation overlies the Tierberg Formation,
902 and is overlain by the Kookfontein Formation. This study focuses on Fan 4. Images taken from
903 Google Earth.

904 Fig. 3: Locations of recently cored wells, outcrops, NOMAD well locations used in the study. Fan 4
905 outcrops are marked in white. Images taken from Google Earth.

906 Fig. 4: Representative outcrop photographs of observed sedimentary facies. A: Structureless thick-
907 bedded sandstone (F1). Person for scale (~ 1.7 m); B: Structured medium-bedded sandstone (F2). C:
908 Hybrid bed (F4) with lower clean division and upper mudstone clast –rich division, Lens cover as
909 scale (~7 cm diameter); D: Thin-bedded heterolithic strata (F6). Logging pole for scale (10 cm
910 increments); E: Thin-bedded siltstone (F7) and mudstone. Lens cover for scale (~7 cm diameter); F:
911 Mudstone (F8) horizon overlain by sandstone. Logging pole for scale (10 cm increments).

912 Fig. 5: Representative core photographs of observed facies. A: Structureless sandstone (F1); B:
913 Structured sandstone (F2); C: Banded sandstone (F3); D: Hybrid bed (F4) with lower clean sandstone

914 division and upper argillaceous sandstone division; E: Debrites (F5); F: Heterolithic package (F6); G:
915 Siltstones (F7); H: mudstone (F8).

916 Fig. 6: Isopach and paleocurrent maps for A. Lower and B. Upper Fan 4. Contours are in meters.
917 Paleocurrent roses represent data collected during the study, whereas paleocurrent arrows
918 represent data from previous work based on Hodgson et al. (2006).

919 Fig. 7: Correlation panels of Fan 4. Top: Correlation of a S-N transect from Bloukop (BK) to Isle of Sky
920 (Ios). Bottom: SW-NE correlation from Klipfontein (Kf) to Isle of Sky (Ios). The base of the mudstone
921 and siltstone interval (black unit) that separates the Lower and Upper Fan 4 is used as a datum.
922 Pinchout of lobes 1-5 of the lower Fan 4 are indicated by black-arrows and their plan-view
923 distribution is shown in Figure 10.

924 Fig. 8: A: Hierarchical model of Fan 4. Location of panel is marked in Fig. 3. Fan 4 consists of two
925 sand-prone divisions that are separated by a thin-bedded heterolithic lobe fringe complex (LC2).
926 Lower Fan 4 comprises one lobe complex (LC1), and upper Fan 4 comprises two lobe complexes (LC3
927 and LC5) and a lobe complex fringe (LC4). Blue square marks zoom-in area of B and C. B: Close-up of
928 the LC2 deposits in the OR well (see Fig. 3 for location). C: Corresponding core photographs.

929 Fig. 9: Representative photographs of lobe successions in the field area. A: Lobe fringe deposits of
930 lower Fan 4 overlain by lobe axis and off-axis deposits of upper Fan 4. Person as scale (~1.7 m); B:
931 Lobe fringe deposits of lower Fan 4 overlain by lobe axis and off-axis deposits of upper Fan 4 C:
932 Lower Fan 4. Hybrid beds are separated by thin-bedded siltstone successions. Person as scale (~1.7
933 m). D: Thick-bedded lobe axis deposits of upper Fan 4. Person as scale (~1.7 m).

934 Fig. 10: Facies distributions and paleogeographic reconstruction for Lower Fan 4, which comprises
935 one lobe complex (LC1) that prograded northward. Black lines indicate the location of lobe-scale dip
936 and strike correlation panels in Figure 12. The green line indicates the location of the Los Kop

937 outcrop area of Hodgson et al. (2006), whereas blue and purple lines mark the location of
938 correlation panels in Figure 7, as do lobe numbers.

939 Fig. 11: Well core log through Fan 4(NS3; see Fig.2). The lower lobe complex of Fan 4 comprises
940 solely thin-bedded heterolithic deposits, siltstones and mudstones, which represents stacked lateral
941 lobe fringe successions. The upper division of Fan 4 shows consists of interbedded structureless
942 sandstone, hybrid beds and heterolithic packages.

943 Fig. 12: Dip and strike facies transitions in individual lobes within LC1 of Fan 4. A: Strike section in the
944 Gemsbok Valley (see Figure 10 for location). Lithology changes from structureless sandstone to
945 structured sandstone to heterolithic deposits. B: Dip section on the Sout Rivier area (see Figure 10
946 for location). Lithology is dominated by structureless sandstone, hybrid beds and siltstone.

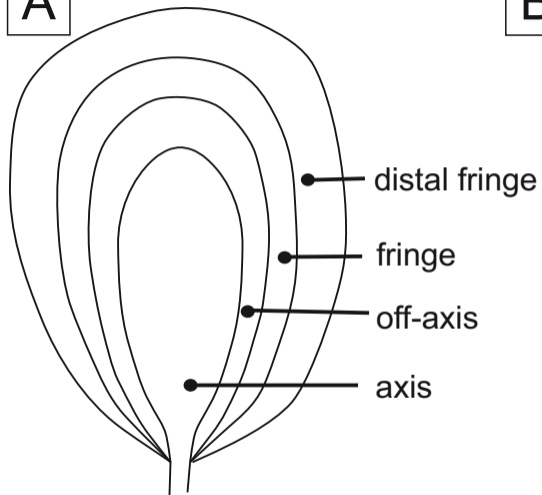
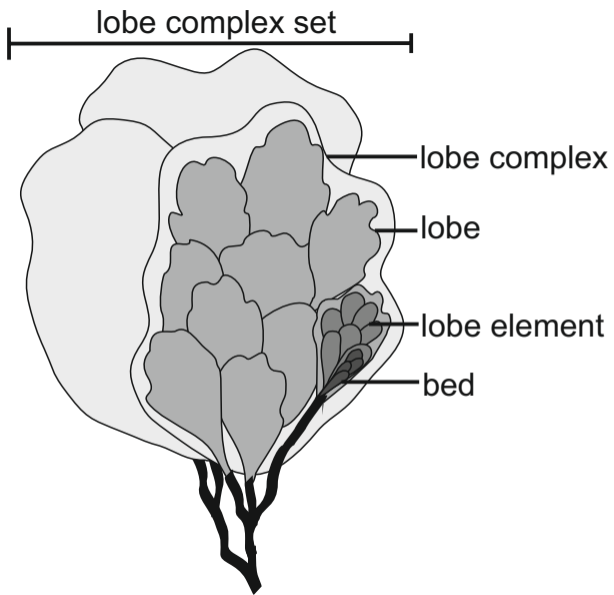
947 Fig. 13: Correlation panels of stacked frontal lobe fringes around Katjiesberg in LC3. A: Location of
948 the correlation panels at Katjiesberg and paleogeography of the Upper Fan 4. B: Areal correlation of
949 four pinch-out fingers and zoom into the northwestern-southeastern part of the correlation panel
950 with sedimentary facies of the pinch-out fingers. They are composed of structureless sandstone
951 deposits, debrites and siltstone deposits.

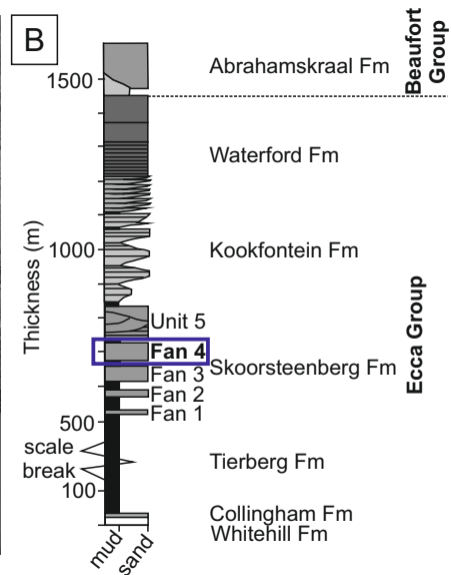
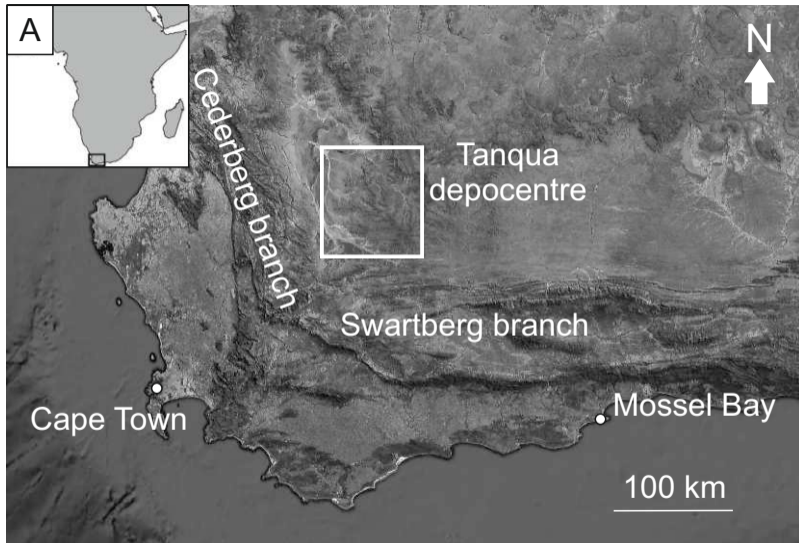
952 Fig. 14: Representative lobe fringe photographs. A: Frontal lobe fringe deposits at Katjiesberg. B:
953 Frontal lobe fringe deposits at Katjiesberg. C: Lateral lobe fringe deposits at Klipfontein. Logging pole
954 for scale. D: Lateral lobe fringe deposits at Hammerkranz. Logging pole for scale.

955 Fig.15: A: Simplified anatomy of frontal lobe fringe deposits. B: Simplified anatomy of lateral lobe
956 fringe deposits. C: Example log showing a vertical section through a frontal lobe fringe in the Sout
957 River area. D: Example log showing a vertical section through a lateral lobe fringe in the Gemsbok
958 East core.

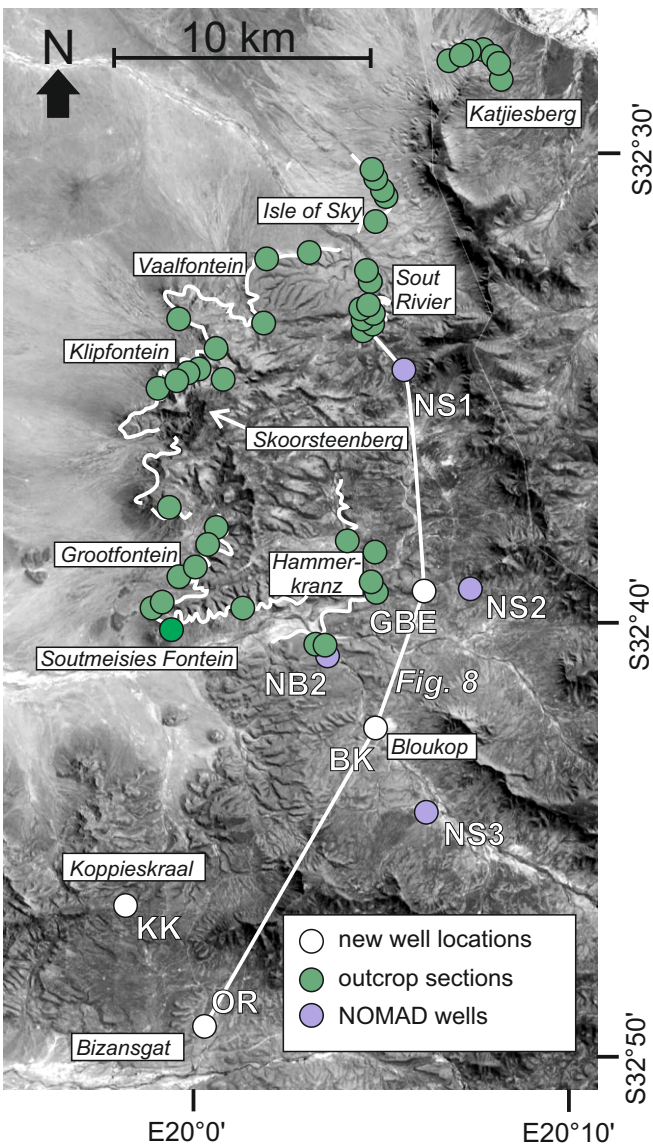
959 Fig. 16 A: Simplified plan view of a lobe marking the distribution of lobe sub-environments and
960 example logs for each sub-environment. B: Dominant flow processes to deposit frontal lobe fringes:

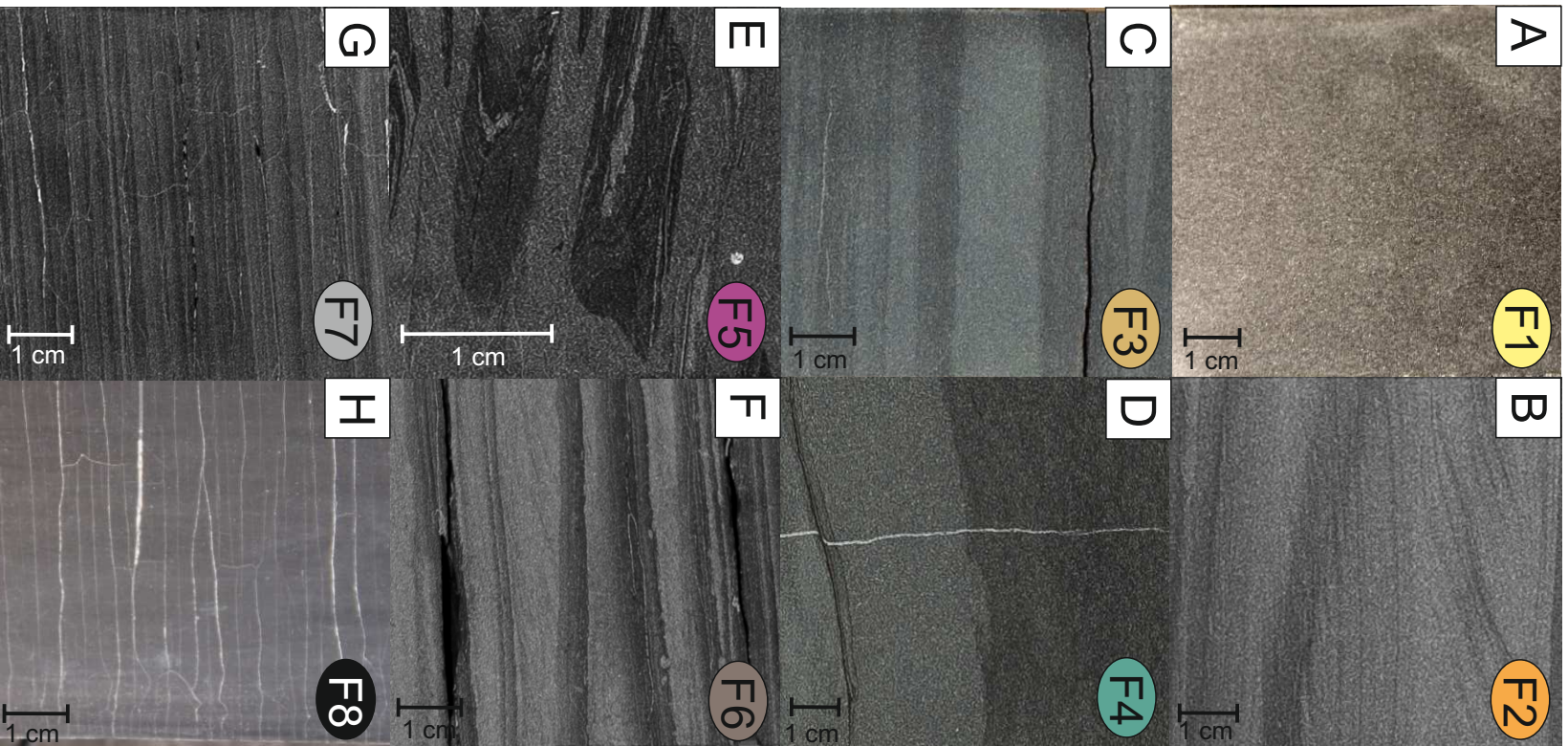
- 961 High-density turbidity currents and strongly stratified flows. C: Low-density turbidity currents and
962 debris flow deposit lateral lobe fringes. C is modified from Kane et al. (in press).
- 963 Table 1. Summary of sedimentary facies of Fan 4.
- 964 Table 2. Recognition criteria of frontal and lateral lobes for outcrop and core.

A**B**

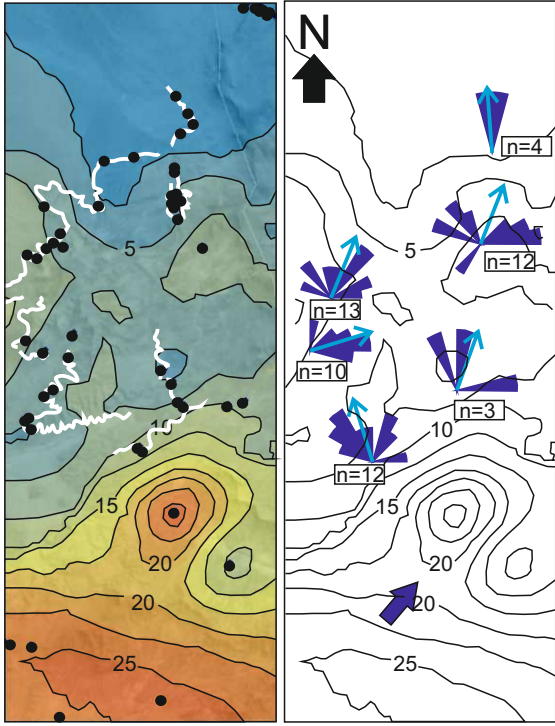




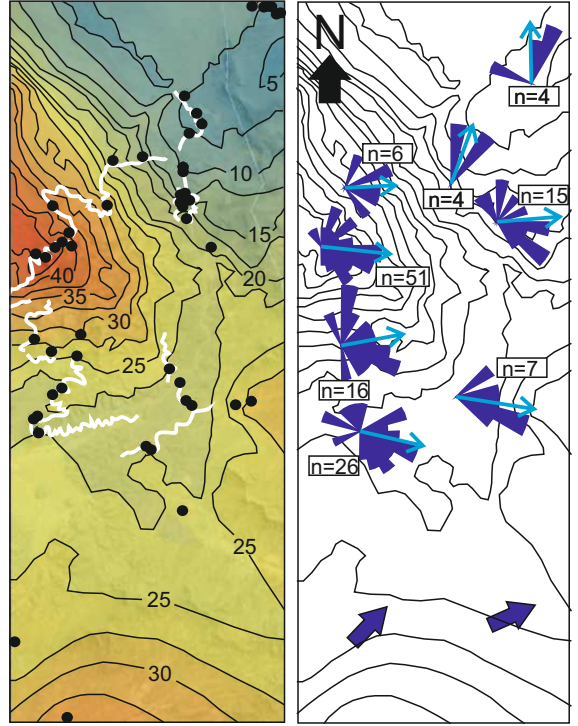




A Lower Fan 4



B Upper Fan 4

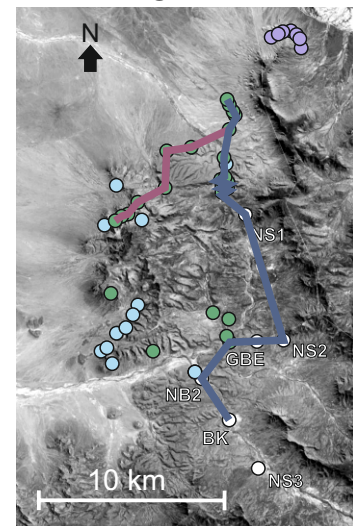
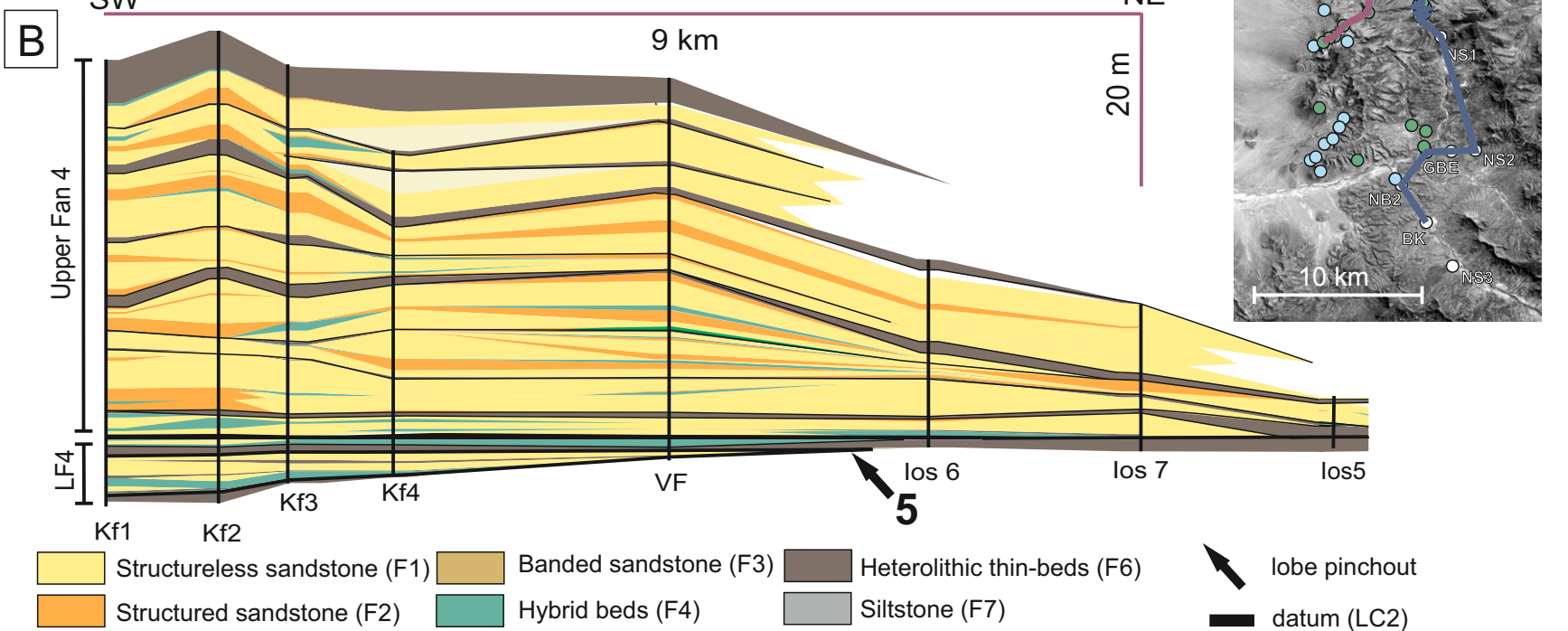
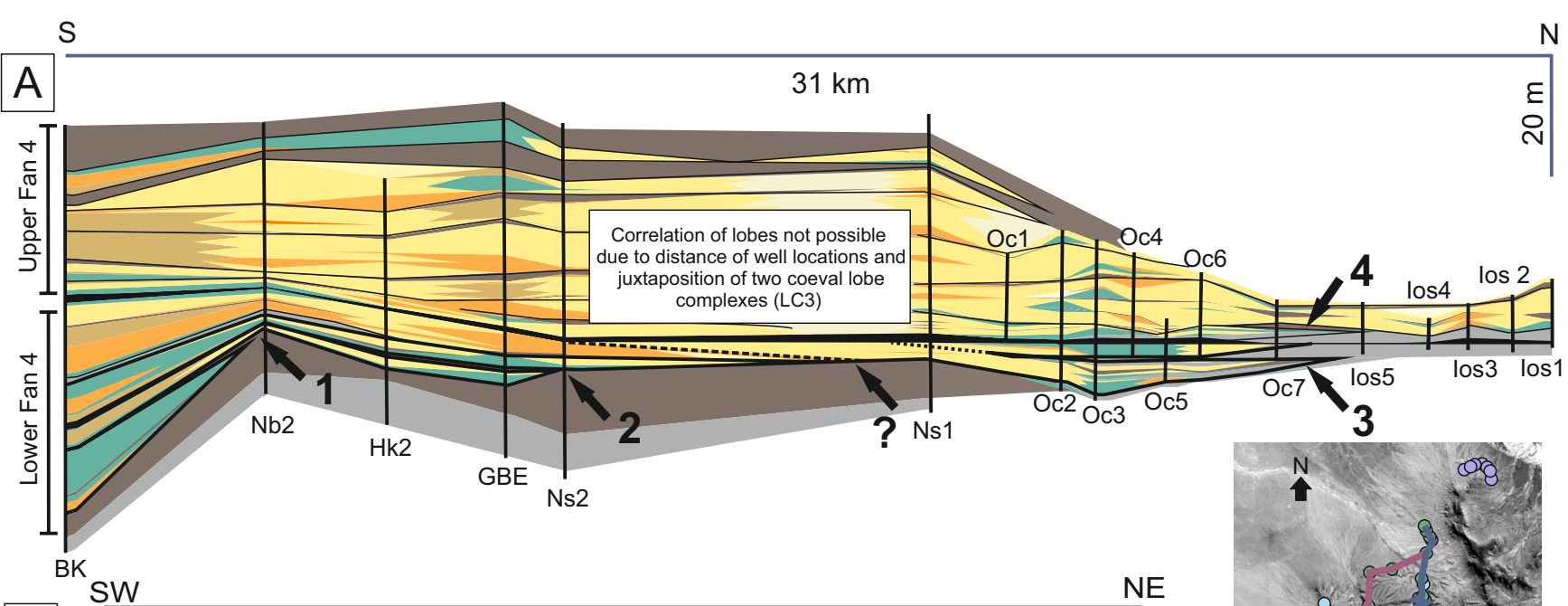


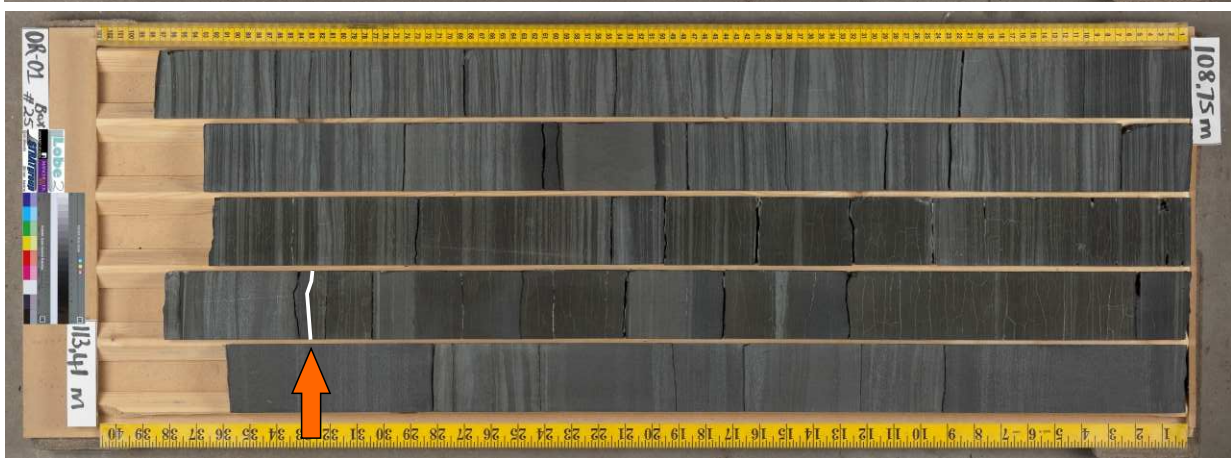
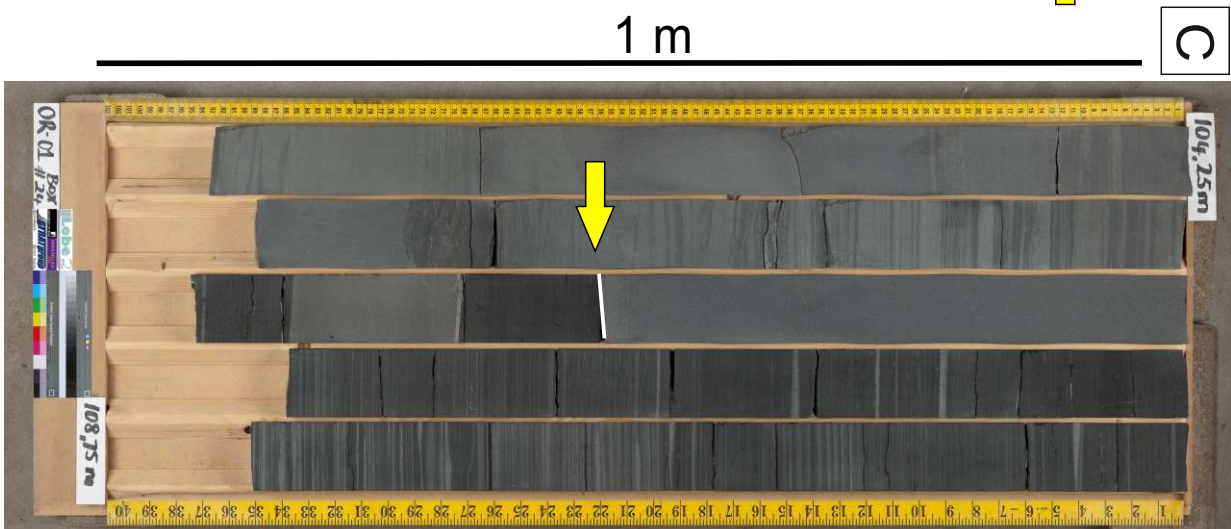
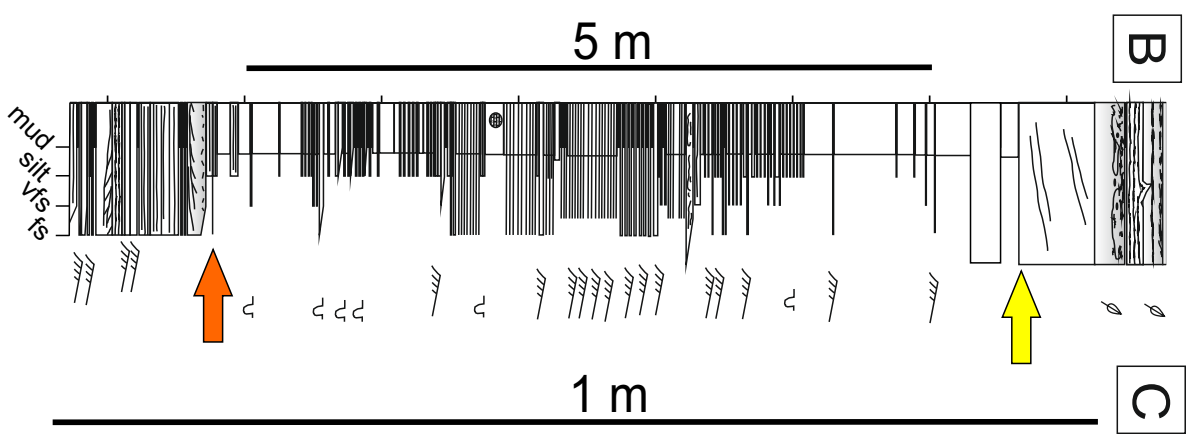
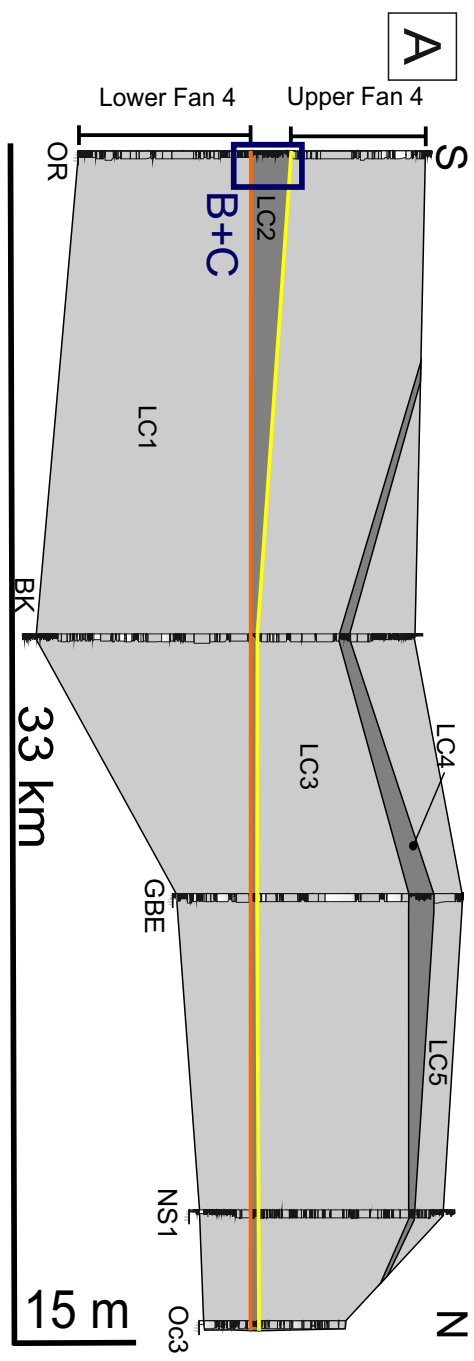
10 km

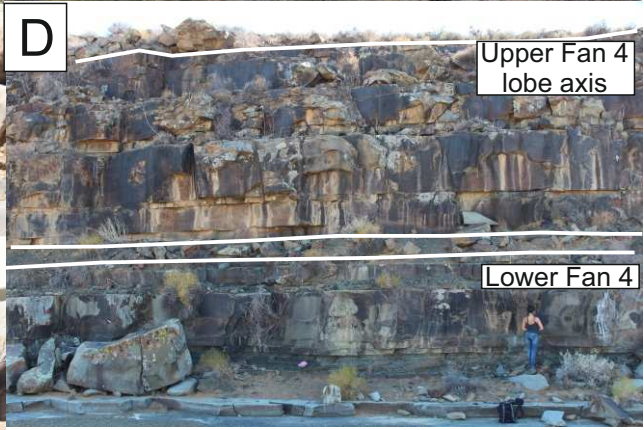
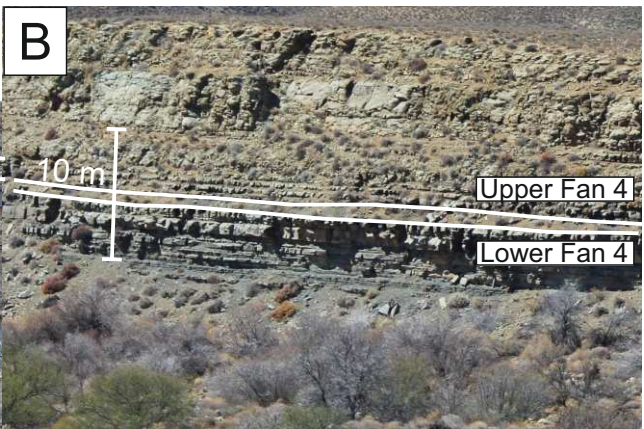
paleocurrent

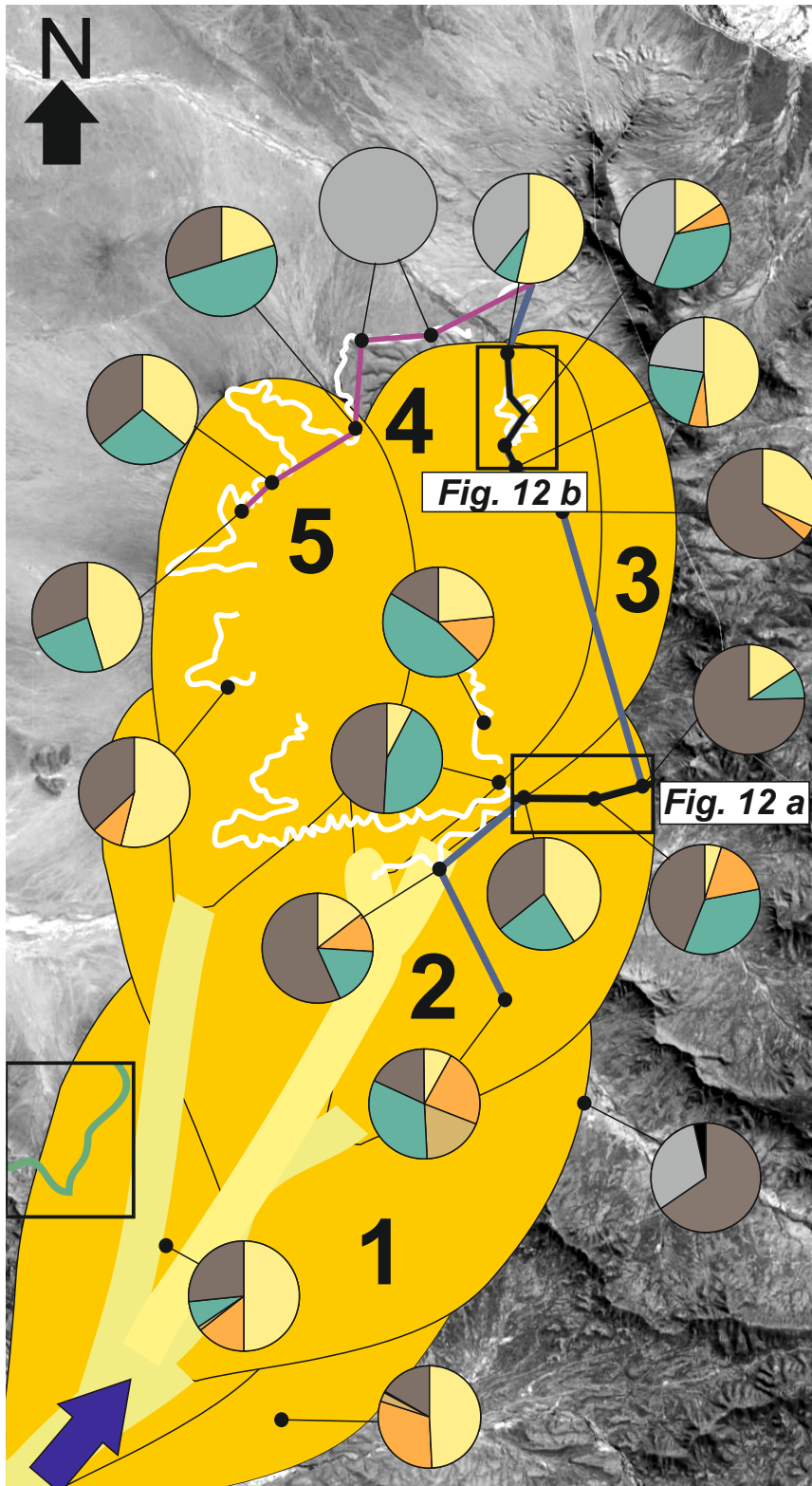
paleocurrent (previous studies)

5 isopach (m)

















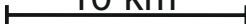


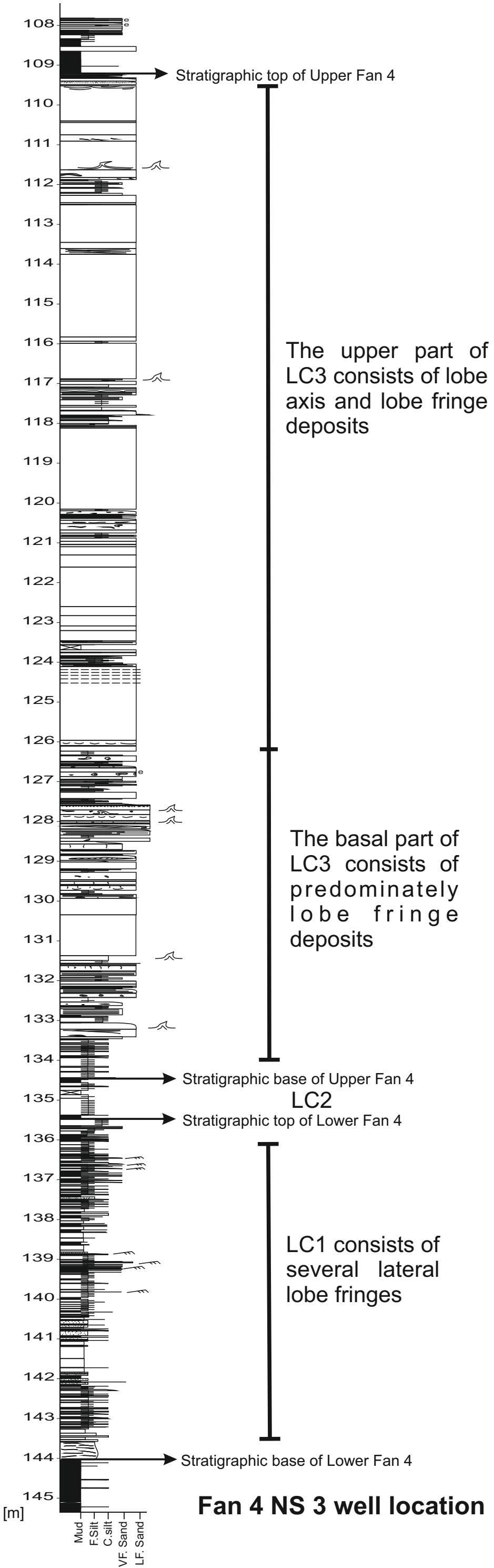
Facies (piecharts)

-  structureless sandstone (F1)
-  structured sandstone (F2)
-  banded sandstone (F3)
-  hybrid beds (F4)
-  heterolithic thin-beds (F6)
-  siltstone (F7)
-  claystone (F8)

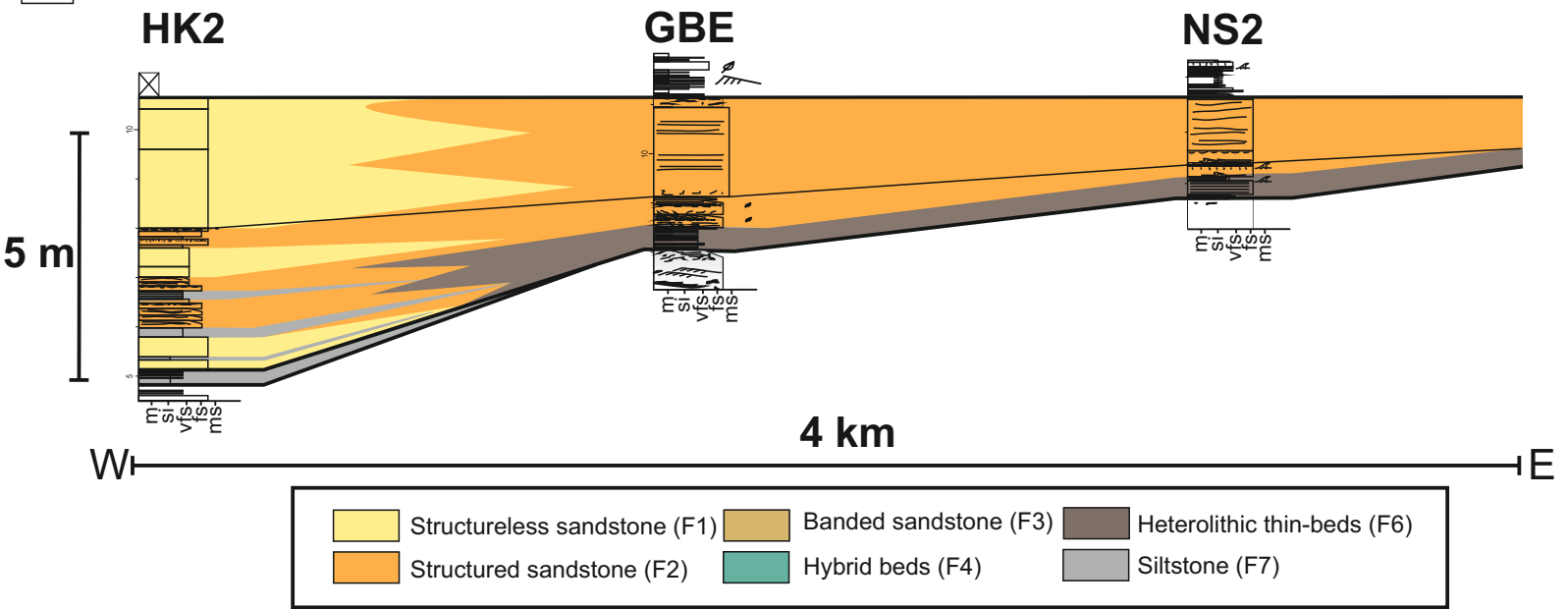
Lobe reconstruction

-  mean paleocurrents
-  correlation panels Fig. 12
-  Los Kop outcrop
-  S-N correlation panel (cf. Figure 7)
-  SW-NE correlation panel (cf. Figure 7)
- 1** lobe number (cf. Figure 7)

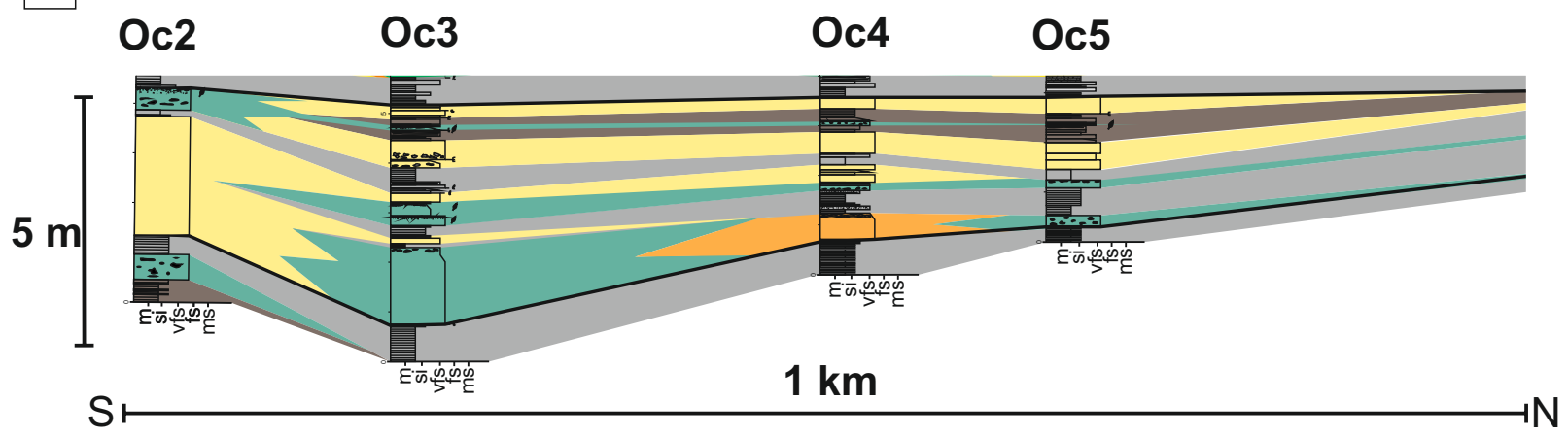
 10 km

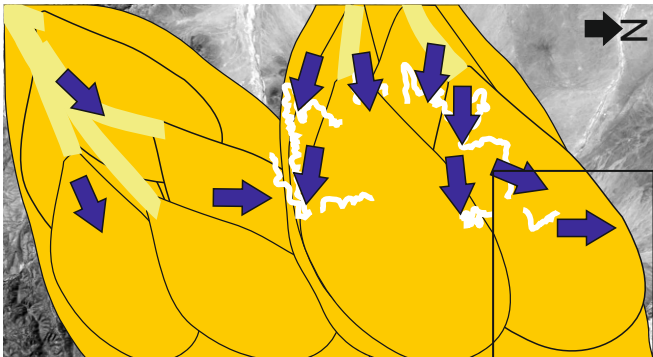
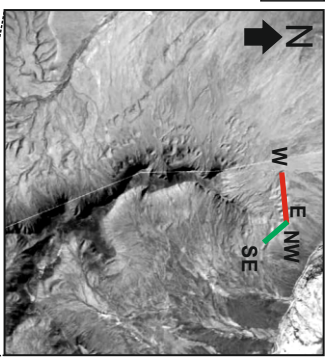
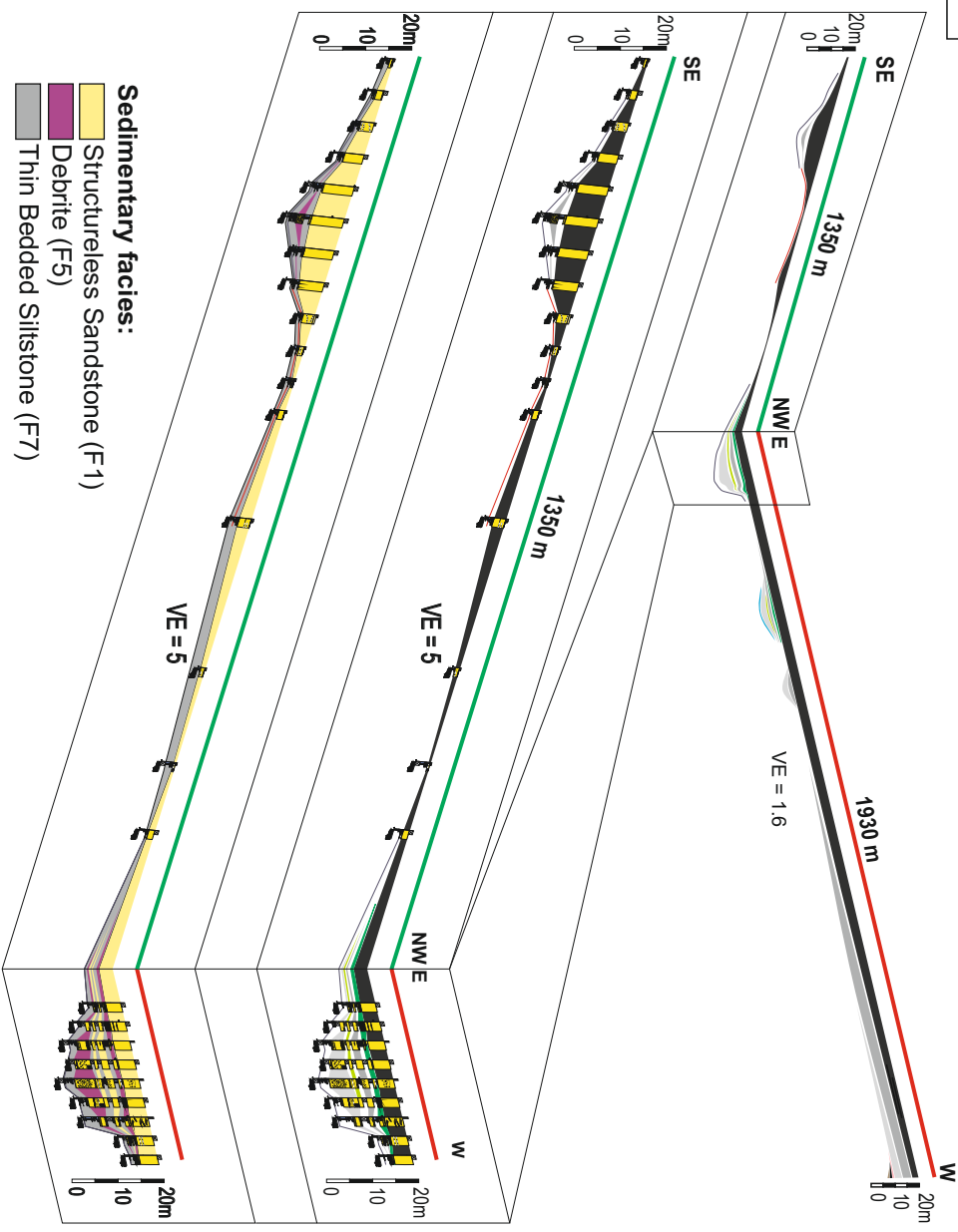


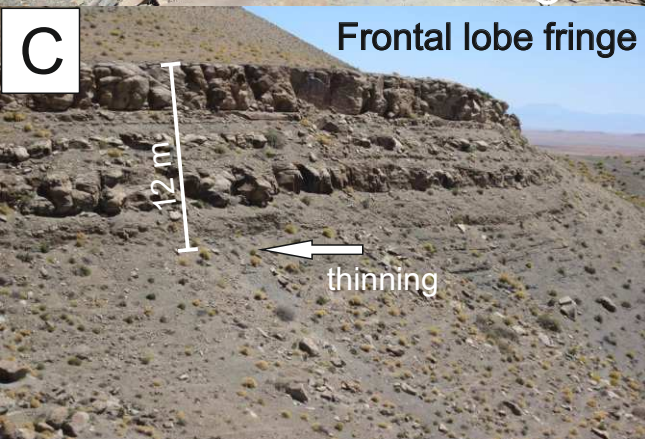
A Oblique strike section from Hammerkranz to NS2

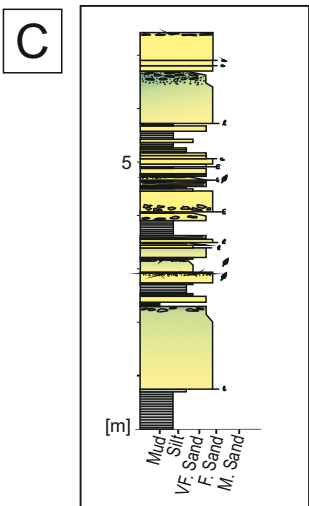
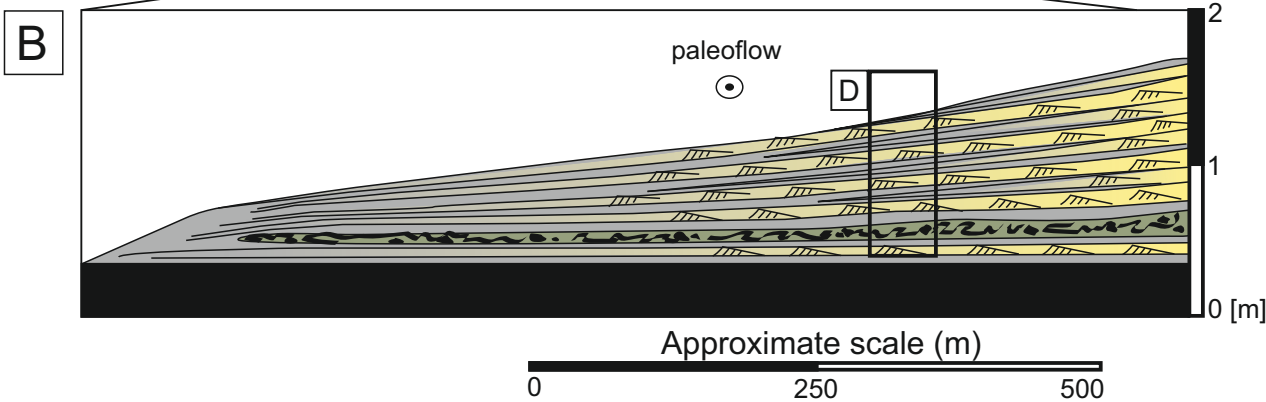
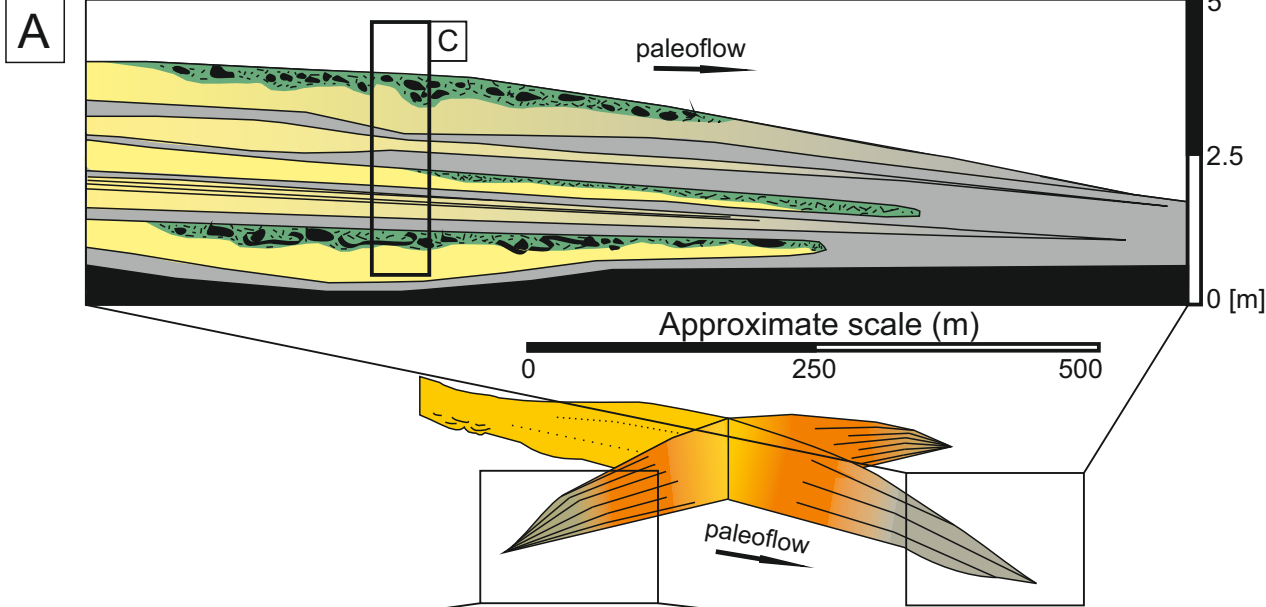


B Dip section in the Sout Rivier area

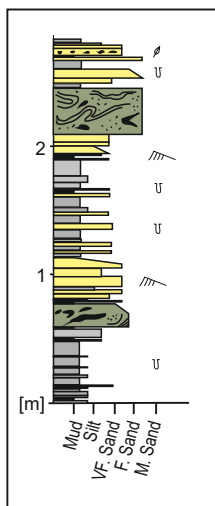


A**B**





example log through Sout Rivier



example log through GBE

Lobe environments

- lobe axis
- lobe off-axis
- lobe fringe

Sedimentary facies

- sandstone
- siltstone
- debrite
- debritic division
- claystone

